Basin Research
IAS EAGE

Geometry and Kinematics of Salt-detached Ramp Syncline Basins

Journal:	*Basin Research*
Manuscript ID	BRE-148-2017
Manuscript Type:	Original Article
Date Submitted by the Author:	20-Dec-2017
Complete List of Authors:	Muniz Pichel, Leonardo; University of Manchester, Basin Studies and Petroleum Geoscience Research Group Peel, Frank; Bureau of Economic Geology, Jackson School of Geoscience Jackson, Christopher; Imperial College, Earth Science & Engineering Huuse, Mads; University of Manchester, School of Earth, Atmospheric and Environmental Sciences
Keywords:	tectonics and sedimentation, salt tectonics, ramp syncline basin, translation, Santos Basin, base-salt relief, minibasins

Note: The following files were submitted by the author for peer review, but cannot be converted to PDF. You must view these files (e.g. movies) online.
Model 1.gif Model2.gif Model3.gif Model4.gif

Geometry and Kinematics of Salt-detached Ramp Syncline Basins

1. Introduction

Ramp-syncline basins (RSBs) are common features in extensional basins, being first recognized in the Gulf of Lyon, offshore France (e.g. Benedicto et al. 1999; Sanchis and Séranne, 2000) and the Kvamshesten Basin, onshore Norway (Osmundsen et al. 2000). They were initially described through conceptual (Gibbs, 1984) and physical models (Ellis and McClay, 1988; McClay, 1990, 1996; McClay and Scott, 1991), as being formed above the hangingwall of ramp-flat extensional faults whose basal detachments dip in the direction of tectonic transport. The hanging wall is warped down above the ramp to create a local basin. As the hangingwall block moves, the locus of subsidence (located above the footwall ramp) remains fixed in space, but its previous sediment fill is progressively moved away from it, producing a characteristic asymmetric, shingled stratal unit (Fig. 1a-b).

A second type of RSB has been identified above salt-detached systems in which the base of the moving unit is a salt layer (Fig. 1c-d) (e.g. Kwanza Basin, Angola, Peel et al. 1998; Marton et al. 1998; Jackson et al. 2001). Building on these studies, Jackson and Hudec (2005) reviewed the processes and kinematics of RSBs on the Angolan margin using highly schematized sections and 2D seismic data. These authors described salt-detached RSBs as being formed by translation of sediments above a salt layer with a basinward-dipping ramp at its base (Fig. 1c-d). Movement over the base-salt ramp generates downwarp of the supra-salt carapace, creating accommodation. Moreover, translation over two or more base-salt ramps can generate vertically stacked RSB systems (Jackson and Hudec, 2005).

Both the extensional and salt-detached RSBs are characterized by an asymmetric synclinal depocentre defined by a basinward-dipping axial-trace (Fig. 1) (Jackson and Hudec, 2005). Thus, sediment layers within RSBs typically dip in the opposite direction to tectonic transport, defining “pseudo-clinoforms” (Fig. 1). In settings where the background sedimentation rate ($\dot{A}$) is low, the top and bottom bounding surfaces of the RSB growth package take the form of diachronous unconformities. The basal boundary is an onlap surface whereas the top boundary is defined by offlap/toplap geometries. In settings where the background sedimentation rate ($\dot{A}$) is relatively high, these surfaces are expressed as diachronous boundaries across which the sediment thickness abruptly changes from expanded within the RSB, to normal thickness outside of it (Fig. 1)

The dip of the depositional axial-trace defines relative ratios of aggradation ($\dot{A}$) and translation ($\dot{T}$) rates (Jackson and Hudec, 2005). Gently-dipping axial traces indicate low $\dot{A}/\dot{T}$ whereas steeply-dipping axial traces indicate high $\dot{A}/\dot{T}$. This ratio tends to increase through time as translation rates usually decrease due to salt thinning and thickening of the overburden (Jackson and Hudec, 2005). Although geometrically similar, extensional and salt-detached RSBs have important differences in terms of stratal architecture, processes and depositional settings that will be addressed in detail in this study.

The geometry and stratigraphy of RSBs can provide important information on the evolution of sedimentary basins. They present an excellent and continuous record of the translation history revealing total duration, displacement distance, speed, and direction (Hudec and Jackson, 2005). With stratigraphic age control of intra-RSB intervals, it is possible to identify whether translation rate was uniform or time-variant, allowing accurate estimates of overburden translation and deformation rates on salt-detached gravity-driven systems (Jackson and Hudec, 2005). This can be extrapolated to more structurally complex domains, such as the updip extensional and downdip contractional provinces, where strain restoration and kinematic analysis can be problematic (Jackson et al. 2014).

Furthermore, in regions where available data do not allow clear imaging of the base-salt surface or pre-salt stratigraphy, the identification of RSBs may indicate the presence, geometry and location of pre-salt highs, as RSBs updip edges occur immediately above them (Fig. 2). This may, in turn, assist the identification of hydrocarbon targets in pre-salt highs sealed by the salt layer, which are prolific plays in the deep-waters of South Atlantic basins (Gomes et al. 2012; Flinch, 2014; Mohriak, 2015). RSBs also control slope and abyssal plain deposition and, thus, can influence the distribution of hydrocarbon reservoirs in supra-salt intervals. Salt-detached gravity-driven translation causes a seaward-shift of supra-salt strata, which can result in juxtaposition of supra-salt sandier intervals deposited on the shelf and upper-slope, above mature pre-salt source rocks on the lower-slope and deep-basin (Fig. 2). If a salt weld is formed below the RSB, these supra-salt reservoirs can be charged by hydrocarbon migration from the pre salt section (Rowan 2004; Jackson et al. 2014). Wherever RSBs are present, one cannot fully understand supra-salt stratigraphic architecture without understanding the kinematics of RSBs.

Despite the notable value for both academia and hydrocarbon exploration, there has been little further research on the subject since Jackson and Hudec (2005). There has been no investigation of RSBs 3D kinematics and stratigraphic architecture, or physical and numerical modelling. Very few studies documented RSBs outside their type-area in the Kwanza Basin: Rowan (2014) in the Red Sea and Dooley et al. (2017) in the Campos Basin, Brazil. Nevertheless, RSBs have been shown in previous works without being explicitly recognized (Alves et al. 2017; Jackson and Hudec, 2017).

Here we present the first ever documentation of RSBs in the Santos Basin, Brazil, providing for the first time a detailed analysis of their 3D stratigraphic architecture and kinematics. We present seismic sections and thickness maps of the RSBs mapped in the Santos Basin and, then, compare their geometries with models that simulate cover translation above a salt detachment with variable topography and thickness. These models provide a more comprehensive and realistic evolution of RSBs, as they treat the detachment as a volume of deforming viscous material (Fig. 1d-f), rather than a discrete undeformable surface (Jackson and Hudec, 2005). This allows us to evaluate the role of diapirism and salt flux variations on RSB evolution. Ultimately, this work aims to improve our current understanding of RSBs and to work as a guide for the identification and analysis of these systems in other settings and basins.

2. Tectono-Stratigraphic Framework of the São Paulo Plateau

The São Paulo Plateau (SPP), Santos Basin (Fig. 3), is an area of thick Aptian salt characterized by prominent intra-salt layering (Fiduk and Rowan, 2012; Jackson et al. 2014; 2015) and a complex, polygonal pattern of salt diapirs (Guerra and Underhill, 2012; Jackson et al. 2015). The area is a prolific hydrocarbon province with discoveries on both pre- and post-salt intervals, including some of the largest oil discoveries in the last decades (e.g. Tupi and Iracema fields) with reserves over 5 bbl in pre-salt structural highs (Mohriak et al. 2012).

The basin is characterized by a series of NE-oriented graben and half-graben formed during late Barremian-early Aptian rifting. These basins are filled by non-marine clastic strata and overlain by shallow-marine carbonates (Meisling et al. 2001; Modica and Brush, 2004; Karner and Gambôa, 2007; Mohriak et al. 2008, 2009; Contreras et al. 2010). During the late Aptian, fault activity was reduced and a 1 - 2.6 km thick post-rift salt succession was deposited (Davison et al. 2012). During the early Albian, the Santos Basin experienced fully marine conditions due to thermally-induced subsidence and eustatic rise, which resulted in widespread deposition of a carbonate-dominated succession, in the study are expressed as a fine-grained, marl-dominated succession (Modica and Brush, 2004). During the latest Albian, thermal and isostatic subsidence tilted the basin south-eastward, inducing gravity gliding and the development of an array of thin-skinned, predominantly seaward-dipping salt-detached normal faults that dismembered the Albian carbonate platform into extensional rafts updip of the study area (Demercian et al. 1993; Cobbold et al. 1995; Mohriak et al. 1995; Guerra and Underhill, 2012; Quirk et al. 2012).

During the Cenomanian-Turonian, drowning of the carbonate platform in response to a rapid eustatic rise and thermal subsidence resulted in extensive deposition of shales and marls in the study-area (Modica and Brush, 2004). Throughout the Late Cretaceous to Paleocene, and despite the continued eustatic rise, sedimentation was dominated by siliciclastic progradation due to landward uplift of the Serra do Mar mountain range, with extensive turbidite deposition during the late Campanian (Modica and Brush, 2004). By the end of the Paleocene, sea-level fall resulted in the development of a major regional unconformity, leading to erosion of shelf and slope sediments, and causing their deposition further basinward. Inflated salt on the SPP acted as a topographic barrier to basinward transportation of coarse clastics from the end of the Paleocene onward (Modica and Brush, 2004), resulting in widespread mud deposition.

The SPP is situated at the present-day toe-of-slope, immediately downdip of the Albian extensional domain and the Albian Gap (Fig. 3) (Quirk et al. 2012; Jackson et al. 2015). Some authors suggest regional shortening of the supra-salt cover in the SPP continued throughout the late Cretaceous (Quirk et al 2012; Fiduk and Rowan 2012; Guerra and Underhill, 2012; Alves et al 2017). Others argue that late Cretaceous deformation was dominated by salt inflation (Jackson et al 2015; Dooley et al 2015). However, there has been no study regarding the aspects of salt-related translation in the area so far.

3. Methods

3.1. Seismic Interpretation

This study uses a zero-phase processed, time-migrated, 3D seismic reflection dataset that covers 20,122 km^2 of the SPP, Santos Basin, Brazil. Inline (west-east) and crossline (north-south) spacing is 18.75 and 25 m, respectively. Vertical sampling interval is 4 ms two-way time travel (ms TWT) and total record length analysed is 5500 ms TWT. The survey display follows the Society of Economic Geologists normal polarity, where a downward increase in acoustic impedance is represented by a positive reflection event (white on seismic sections) and a decrease in acoustic impedance by a negative event (black on grey-scale seismic section) (Brown, 2011).

The dominant frequency in the Aptian salt is c. 30 Hz and the average interval velocity is 3.4 km/s, which yields a vertical resolution around 25-30 m. The relatively lower velocity of the salt compared to pure halite is due to the intra-salt lithological heterogeneity and presence of acoustically slower potash intervals (Jackson et al. 2015). Overburden sediments have a similar frequency of c. 31 Hz and a lower average interval velocity (c. 2.0 km/s), which, together result in a much finer vertical resolution (c. 15-20 m) coarsening with increasing depth and increasing velocity. Horizontal resolution is twice the seismic line spacing (i.e., 37.5 m in the E–W direction and 50 m in the N–S direction) (Jackson et al 2015).

In order to understand the 3D kinematics and tectonostratigraphic evolution of RSBs, 3D seismic mapping of key internal horizons was conducted using in in-lines, cross-lines, and in strike- and transport-parallel sections to obtain accurate estimates of the translation history of these systems. TWT structure maps for top-salt (Fig. 4) and key surfaces within the RSBs were produced to generate thickness maps of key stratigraphic intervals.

The study did not involve the use of primary well data, or independent picking of horizon tops in wells. Intra-RSB horizons were chosen as the most distinctive positive reflections with high amplitude and lateral continuity. Identification of key seismic stratigraphic surfaces, such as the base and top salt, top Albian, and the intra-Paleocene unconformity, was based on previous publications (Fiduk and Rowan, 2012; Guerra and Underhill, 2012; Jackson et al. 2015; Alves et al. 2017).

3.2. Base-salt Map

It was vital to have a detailed base-salt map in order to match the observed RSBs to the base-salt topography responsible for their formation. Although, the top and base-salt surfaces were readily identified and interpreted in TWT; the presence of a thick, deformed evaporite layer, whose velocity is higher than the overlying sediments, introduces distortion of the base-salt and pre-salt section such that the real structure is obscured by velocity pull-ups. Although, in places, syn-rift structures (i.e. normal faults and wedge-shaped intervals) helped constraining pre-salt structures (Figs. 6-7), in other areas these structures could not be readily identified in an unadjusted TWT base-salt map.

Publically available depth-maps (e.g. Alves et al. 2017) do not cover the entire study area nor do we have access to a reliable, high-resolution velocity grid to create maps by conventional depth-conversion. Instead, we developed a reliable and applicable base-salt structure map (Fig. 5) by stretching the thickness of salt by a factor of 1.61 and shifting everything below salt accordingly. This is equivalent to a static correction, in which the velocity of salt is reduced to 61% of its natural value. The appropriate substitution factor was obtained by iteration to find the value that best removes observed pull-up. Finally, a gentle spatial smoothing factor was applied to remove the effect of non-vertical ray paths, which created local high-frequency spikes under the steeply-dipping flanks of salt bodies (Jones and Davison, 2014). The resulting map is in TWT, not depth, and it represents where the base-salt reflection would be if the salt were replaced by an equivalent thickness of sediment.

The best indicator that the process was effective is that the resulting map (Figure 5a) shows no discernible imprint of the overlying salt structure, and it compares favourably to depth-maps such as that presented by Alves et al. (2017). Four major base-salt highs are identifiable on the map; each bounded updip and downdip by base salt ramps (Fig. 5). This result compares well with the interpretations shown by Davison et al. (2012) and Alves et al. (2017), both of whom used depth data.

4. Ramp-Syncline Basins in the Santos Basin, Brazil

Several series of simple and stacked RSBs were identified above thick salt (1.5-2 km) in the Sao Paulo Plateau, Santos Basin, distributed above and basinward of the main base-salt steps in the area (Figs. 4-5). These basins trend NNE to NE (Figs. 5) and are composed of 9-20 km wide by 15-35 km long continuous panels of landward-dipping and thickening strata that become younger landward (Figs. 6-10). Base-salt steps trend NNE to NE, parallel to the RSBs, although the northernmost high trends NNW, oblique to them (Fig. 5) (H2 of Alves et al 2017). In this study, we present the 5 least deformed, largest, and thus best imaged examples of RSBs in order to analyse their 3D kinematics, tectono-stratigraphic evolution, and interaction with diapirism and base-salt structures.

The RSBs are characterized by asymmetric sigmoidal strata dipping and expanding landwards towards a diachronous basal boundary, being capped by a diachronous top unconformity (Figs. 6-8). Their depositional axial-trace (red dashed line) dips mainly basinward, becoming progressively steeper at the uppermost strata, landward (Fig. 6-7). However, viscous salt drag and synchronous diapirism can bend and rotate RSB intervals, switching the dip direction of their axial-trace (Fig. 8).

These systems contain stratigraphic successions up to 700 ms (~800 m) thick (Fig. 8); with an average vertical thickness of 400 ms (450-500 m, Fig. 7), which corresponds to only

20-40% of total post-salt succession. However, this does not represent the true stratigraphic thickness of the RSB fill as these strata have been rotated by a combination of translation (>20 km) and diapirism (Figs. 6-10). Thickness maps of intra-RSB intervals indicate a minimum true stratigraphic thickness varying from 1,670 ms (~ 1,900 m) in RSB 3 (Fig. 8) to 2,130 ms (~ 2,400) in RSB 4 (Fig.10).

In the majority (85%) of RSBs identified, the first onlapping strata occur against the top Albian interval (Figs. 6 and 8-10), characterized by a broadly isopachous section, 300-400 ms (c. 300-400 m) thick, of continuous and low-amplitude reflections defined at the top by distinctive high-amplitude positive reflections (Guerra and Underhill, 2012; Jackson et al. 2015). In the other 15% of RSB panels, the first onlaps are against younger, late Cretaceous strata (Fig. 7). Our interpretation suggests that this occurs because these systems can be segmented by salt walls and diapirs (Fig. 8-10). In places, horizon correlation along-strike and around the diapirs (Fig. 4) shows that the landward panels are composed of younger strata onlapping a thicker and younger pre-translation section (Fig. 8), relative to their basinward equivalent panel. This indicates these panels are genetically linked, comprising a single RSB formed by post-Albian translation above the same ramp (Fig. 11a-b), and that they were subsequently separated by syn- to post-translation diapirism. Another evidence of viscous salt drag and basinward translation in these systems is the development of intra-salt basinward-vergent shear zones (Figs. 6 and 8).

In the north-central and northeast portions of the SPP, RSBs have a distinctly different geometry compared to those further south. They are characterized by stacked onlap surfaces and ramp-syncline strata (Figs. 9 and 10), formed by simultaneous cover translation above two or more base-salt ramps (Jackson and Hudec, 2005). Each of the stacked RSBs develops by strata translation, rotation, and bending above a single base-salt step. The lower or landward RSB forms by translation above the landward ramp, whereas the upper or basinward RSB forms by translation above the basinward ramp (Figs 9, 10 and. 11c). If the distance between the base-salt ramps is smaller than the amount of translation in the system, the updip portion of the basinward RSB overlaps the downdip portion of the landward RSB, generating a set of stacked RSBs (Figs. 9-10). Intuitively, the distance between steps is inversely proportional to the width of the stacked RSB section. Deposition occurs simultaneously within both stacked RSBs, so the first and last deposited strata and equivalent onlap points in each RSB have the same age and, accordingly, the amount of translation in each RSB is the same (see models, section 4.3) (Jackson and Hudec, 2005).

The stratigraphic architecture of stacked RSBs is similar to the individual systems described previously (Figs. 6-8), with landward-dipping sigmoidal strata defined by a basinward-dipping axial trace (Figs. 9 and 10). In both cases, stratal termination can vary along dip and strike. Thus, we present a summary of RSB stratigraphic architecture and terminations for both the simple and stacked systems (Fig. 11).

Lower boundaries are generally characterized by a well-defined, diachronous onlap surface that becomes younger landward (Figs. 8-10). Apparent downlaps are typical of the lowermost RSB fill, which has been progressively rotated during translation, whereas the original onlap relationships are most easily discerned for the younger landward packages (Figs. 6-10). We thus interpret the apparent downlaps as being originally formed as onlaps against paleo-bathymetric highs and/or diapirs above base-salt ramps. These terminations dominate where strata are older and consequently have been translated and rotated further. Elsewhere, the basal boundary is also defined by transition from thicker, landward-dipping section to a drape interval at regional dip (Figs. 8-10 and 11b-c).

Upper boundaries also become younger landward and are defined in places by erosional truncation, most commonly in the downdip part of the system where strata are usually steeper (orange to blue horizons, fig. 7). Steep stratal dips and erosional truncation are possibly caused by a combination of: i) uplift due to salt drag (see model in Fig. 8) and/or salt inflation at the edge of the RSB (not modelled); and ii) a higher degree of translation and rotation of older RSB strata. Elsewhere, the upper boundary is defined by toplaps (lilac horizon, fig. 7) or, usually in the updip portions of the system, by an abrupt transition from thin, draping section with an overall regional dip to a thicker section that dips more steeply than regional (light orange horizon, Fig. 7).

This landward shift from abrupt to subtle, transitional limits along the upper and lower boundaries of the RSBs (Fig. 11b) is explained by an increase in the ($\dot{A}/\dot{T}$). This is evidenced by the landward steepening of the depositional axial-trace in areas where the RSBs are less folded (Fig. 6-10). Additionally, as the RSB evolves and the $\dot{A}/\dot{T}$ increases, the overburden becomes progressively thicker such that loading and salt expulsion can act as a secondary control on RSBs evolution. Thus, salt expulsion and diapirism occur in tandem with translation and RSB development (Jackson and Hudec, 2005), as seen in portions of our seismic examples where RSBs have a more symmetric geometry and salt has drastically thinned beneath them (SE edge of RSB 3, Fig. 8).

Vertical juxtaposition of stacked RSBs can complicate their stratal terminations. The unconformity bounding the top of the lower RSB forms the basal onlap surface of the upper RSB along most of the stacked section (Figs. 9-10). However, as in simple RSBs, the boundaries of each stacked system can be defined by transition from steeper, thickened section within the RSB, to thin, draping strata away from it (Figs. 9 and 10b). This can result in the development of a thin drape interval separating the lower RSB top unconformity from the upper RSB onlap surface (Figs. 9 and 10), which typically occurs in their uppermost sections (Fig. 11c).

5. RSB modelling and kinematics

The observations made from seismic interpretation were compared with forward models reproducing what was interpreted as the main process operating in these settings, i.e. cover translation above a thick salt detachment. This comparison allowed us to evaluate the kinematics and processes controlling the development of RSBs and to confirm that the observed geometries were explicable in the framework of the interpreted base-salt topography. In such systems, translation of the cover is accommodated by layer-parallel shearing of the whole thickness of the salt, i.e. Couette flow (Weijermars, 1993; Rowan et al. 2004) as opposed to movement on a fault (McClay, 1990; 1996) or a discrete detachment surface (Jackson and Hudec, 2005).

Modelling was performed using a novel application, SaltDragon©, created in Microsoft Excel©. This application provides a simple but effective 2D model of the stratal geometries produced in RSB systems by simulating viscous salt drag and overburden translation above a thick salt detachment with variable thickness and basal topography. The geometry of the decollement and the rate of sediment accumulation can be adjusted in order to replicate the general form of the natural RSBs observed on seismic data, and to investigate the possible controls on RSB geometry. The application is non-dimensional, i.e. scaling-independent: the computations relate to grid cells, and are valid regardless of the dimension of the grid, or of the vertical scaling factor.

The overburden is offset horizontally, one grid cell per time increment, over the viscous decollement, with an initially uniform top and a base of user-defined irregularity, while the pre-salt interval remains fixed and rigid. The post-salt pre-translation interval is represented by a tabular package and syn-kinematic sedimentation is continuous and at a constant rate through time. After each increment, the overburden is deformed by vertical shear to maintain contact with the top of the salt. The height of the new sediment depositional surface at each point in time is user-defined. The calculated accommodation (space between the new depositional surface and the top surface of the deformed overburden) determines the thickness of new sediment deposited in each increment. There is no compaction and erosion in this model and the depositional surface is presumed to be planar and uniformly dipping, which is likely applicable to the deep-water settings considered in our natural examples. The process is repeated sequentially, creating a complete realisation of the evolution of the system.

The shear strain associated with the layer-parallel shearing within the salt is assumed to be uniform throughout each vertical column (Fig. 12). Thus, where salt is thinner, the total flux of dragged salt is lower than where the salt is thicker and *vice versa* (Fig. 12) (Dooley et al. 2017). As the original salt thickness changes across base-salt topography, the overall salt flux also changes. As a result, parts of the section may experience net loss or gain of salt, resulting in salt thickness variations and subsidence or uplift of the overlying sediments (Fig. 12). This controls the deposition and stratigraphic architecture of syn-kinematic strata, and the development of RSBs.

Because the models begin with a planar top-salt surface; in its initial stages, the generation of subsidence and uplift is entirely due to the effect of salt drag and laterally varying salt flux (Figs. 12a-b). However, as the model evolves, significant topography is created on the top salt surface and a second factor comes into play. The cover, then, moves with a downward component where the top-salt dips in the direction of tectonic transport, and has an upward component where the top of salt dips in the opposite direction (Figs. 12c). This produces components of local subsidence and uplift, in addition to those created by local depletion or increase in salt thickness. An important consequence of this is that regions of local uplift can develop in the downdip side of RSBs even where the cover is moving over a basinward-dipping ramp (Fig. 13c-d).

As the top-salt topography develops, the amount and extent of uplift should progressively increase (Figure 13c-d). In nature, a combination of Couette and Pouiseuille salt-flow would intensify the uplift as salt would be laterally expelled from beneath the RSB resulting in inflation and diapirism at its edges. If the system experiences very large lateral displacement, we would expect the salt layer thickness to become near-uniform, as differential Couette drag tends to progressively even out the initial variation in salt thickness.

We present 4 models where we test the effects of different base-salt topography and variable salt thickness on overburden translation. Model 1 simulates translation above a basinward-dipping ramp and model 2 reproduces translation above a pair of basinward-dipping ramps. In Model 3, we evaluate translation over a landward-dipping ramp and in Model 4, translation over a base-salt high (horst block), with a landward- and basinward-dipping ramp.

Whilst the models appear to reproduce actual geometries observed in salt basins, they do not reproduce the entire kinematics and other salt-related processes that operate in RSB systems, such as diapirism and Pouiseuille-flow driven by differential loading. Also, it makes the assumption that: 1) the overburden neither stretches nor shortens laterally as it moves or, 2) the sediment layer has very little resistance to vertical shear, so there is no salt return Poiseuille-flow component, as would be the case with a more rigid roof. Nevertheless, separating the contribution of one factor alone (entrainment of the viscous decollement layer by drag, modelled as Couette flow) allows us to explore the influence of this important component of salt tectonics. Furthermore, the fact that this approach produces results that are remarkably similar to RSBs observed in both Santos and Kwanza Basins, suggests it is a valid first-order approximation of their dynamics.

5.1. Model 1 (Basinward-dipping ramp)

In Model 1, salt and overburden translate over a basinward-dipping ramp. As salt is thinner updip of the step (Fig. 13), less salt is dragged into the step than out of it (Dooley et al. 2017). This salt deficit results in local salt thinning and cover subsidence (Fig. 12a and 13a-b), and the generation of an asymmetric depocentre above the ramp. As translation continues, previously deposited strata are moved out of the ramp while new sediments are deposited immediately above it. This results in the development of a RSB, characterized by an asymmetric growth interval that dip and expand landwards towards a diachronous basal boundary, being truncated above by a diachronous unconformity (Fig. 13c-d), similar to natural examples from the SPP (Fig. 6).

The axial-trace and bounding surfaces are sub-parallel to each other (Fig. 13d). Initially, they dip gently in the direction of tectonic transport, i.e. basinward (Fig. 13b) but as translation progresses, salt drag and uplift rotate these surfaces, flipping their dip direction, i.e. landward, at the downdip edge of the system (Fig. 13c and d). Because in the model translation and sedimentation rates are constant, this change in geometry happens entirely in response to shear drag and the consequent upward translation and rotation of syn-kinematic strata. In reality, folding and rotation of RSBs internal intervals and surfaces can be even more pronounced due to a combination of: i) variations in $\dot{A}/\dot{T}$, ii) salt expulsion and diapirism, and ii) extension and contraction.

Basal surfaces of salt-detached RSBs are usually diachronous and shingled (i.e. not a discrete surface as in extensional RSBs) as sediments may also be deposited upslope of the RSB in the form of a thin drape fringing the main depocentre (Fig. 13c and d). In our seismic examples, thin drape horizons usually occur at the updip portions of the systems, being usually 1-2 seismic reflections thick (Fig. 9), equivalent to only a few tens of meters.

Model 1 is also run with a higher $\dot{A}/\dot{T}$ to illustrate how varying the relative rates of aggradation and translation produces different RSB stratal architectures (Fig. 14).

Translation rate ($\dot{T}$) is kept constant while aggradation rate ($\dot{A}$) is increased 3-fold (Fig. 14b). When the $\dot{A}/\dot{T}$ is low, the RSB geometry is more asymmetric and its boundaries are defined by abrupt strata terminations (Fig. 14a). Conversely, when the $\dot{A}/\dot{T}$ is high, there is less asymmetry, the synclinal axial-trace is steeper, and strata terminations are characterized by a transition from a thicker, steeper section within the RSB to thinner intervals at regional dip outside of it (Fig. 15b). If $\dot{A}$ is higher than $\dot{T}$, local uplift in the downdip side of the RSB is not enough to generate sea-floor exposure and erosion (Fig.12c and 14b), which in a deep-water setting as in the SPP, could be driven by bottom currents. Although not shown here, variations of sedimentation rate during the development of RSBs can also produce intra-RSB unconformities and offlap terminations.

5.2. Model 2 (Two Basinward-dipping ramps)

Model 2 simulates cover translation above a thick salt layer with two closely-spaced base-salt basinward-dipping ramps (Fig. 15). Basin geometry and evolution above each base-salt ramp is similar to Model 1, such that a landward RSB forms above the landward ramp while a basinward RSB develops above the basinward ramp (Fig. 15b-c). As translation continues, these basins are vertically juxtaposed forming stacked RSBs (Fig. 15c-d) as in our seismic examples (Figs. 9-10). Deposition occurs simultaneously within both RSBs (Fig. 15b-d), which means the first and last deposited strata and respective onlap points in each of the stacked RSBs have the same age and, accordingly, record the same amount of translation (Fig. 15) (Jackson and Hudec, 2005).

The most basinward interval of each RSB corresponds to older strata that have translated further, thus, being more rotated and uplifted by shear drag than younger intervals (Fig. 15). If the aggradation rate is lower than salt movement rate, salt drag results in exposure of the basinward side of each RSB (Fig. 15d), leading to localized erosion, as seen in natural examples (landward and basinward RSBs in fig. 10 and landward RSB in Fig. 9).

417 The width of the exposed area is smaller in the landward RSB, presumably because it is progressively and partially buried by the basinward RSB strata, onlaping onto the landward RSB top unconformity (Fig. 15d).

420 Our model shows that the lower, landward RSB top unconformity acts as the basal onlap surface of the upper, basinward RSB (dashed black line in fig 15d), as seen in seismic examples (Figs. 9 and 10). When the sedimentation rate is lower than the translation rate, the stacked RSBs top unconformities merge landward, and their basal onlap surface merge basinward (Fig. 15). Although there is a level of uncertainty due to the presence of folds and diapirs in the study area, this pattern is seen in portions of RSB 5 (Fig. 10 a-b), where the RSB interval is thinner. When sedimentation rate is relatively higher, a thin drape interval can separate these boundaries (Fig. 9).

428 As seen in the model each RSB finishes landward above the top of its respective ramp (Fig. 15d). This is seen throughout most of our seismic examples (LW ramp and middle ramp RSBs in Fig. 10) although in some areas, diapirism and overburden deformation can laterally offset their landward edge from the top of their respective ramps by up to 1-2 km (Fig. 9). These complexities, however, lead to only a minor amount of uncertainty when compared to the total translation and extent of these systems (see section 4.5) and, thus, are not enough to invalidate translation estimates.

435 **5.3. Model 3 (Landward-dipping Ramp)**

436 Model 3 simulates cover translation above a thick salt detachment with a landward-dipping basal step and generates similar syn-kinematic stratal geometries to Model 1. However, this time, the RSB forms immediately basinward of the step, above a base-salt flat (Fig. 15), instead of above the step as in Model 1 (Fig. 16). As salt moves from an area of thick to thin salt across the ramp, salt streamlines converge so that more salt is dragged into the

ramp than out it (Figs, 12b and 16a-b) (Dooley et al. 2017). This salt surplus results in salt thickening and cover uplift above the step, and generation of accommodation around the salt anticline formed over the ramp.

As translation continues, more salt is fed into the anticline causing it to widen basinward without leaving its original position. Thus, whilst its landward flank remains static, the basinward flank translates and acts similarly to a basinward-dipping ramp forming an asymmetric depocentre above it. Syn-kinematic strata onlap and thicken towards this flank while being progressively rotated and translated basinward (Fig. 16b-c).

The evolution and geometry of the asymmetric growth interval are notably similar to RSBs formed above basinward-dipping ramps (compare Figs. 13 and 16) and to natural examples of RSBs formed above landward-dipping steps (Figs. 7 and 8). These RSBs are composed of shingled sigmoidal strata that dip and expand landward, being located basinward of a landward-dipping base-salt step and above a base-salt flat (Figs. 7 and 8). They are bound on their landward edge by a wide diapir (Fig. 7) or a salt anticline (Fig. 8) that is situated directly above the top of the ramp, as in the model (Fig. 16).

In the model, the salt anticline remains static but, in reality, it can abandon the ramp after reaching enough topography and gravitational instability, being translated downdip while a younger salt structure forms above the ramp. After leaving the ramp, the structure will probably experience extensional reactivation as the system accelerates, as shown in physical models (Dooley et al. 2017) and seismic examples (mid-RSB diapirs in Fig. 9). As the anticline grows and its roof is uplift, outer-arc extension and erosion (not modelled) can thin the roof and allow diapiric piercement as seen in RSB 2 (Fig. 7).

The apparent offset of synkinematic strata across the diachronous onlap surface above the anticline could be erroneously interpreted as a basinward-dipping listric fault (Fig. 15c-d). However, it is clear from natural examples and models that this geometry is entirely formed in response to differential uplift and sedimentation during cover translation. As salt thickens above the ramp, sediments are deposited around the anticline while the area above it remains sediment starved (Fig. 15). As translation progresses and the anticline widens, the landward section is translated over the structure, while the basinward section translates further basinward (Fig. 15c-d). Ultimately, this will result in an apparent offset that is equal to the width of the diapir (Fig. 15c-d), but which is clearly not associated with faulting.

5.4. Model 4 (Base-Salt High)

Model 5 illustrates the development of stacked RSBs formed by translation over a base-salt high akin to a horst block defined by a landward-dipping ramp updip and a basinward-dipping ramp downdip (Fig. 17), as in RSB 5 (Fig. 10). Each step works as in previous models. Translation across the landward step results in salt thickening above the step and development of a RSB basinward of it, whereas translation over the basinward step results in salt thinning and subsidence with generation of another RSB above it. As translation progresses these minibasins overlap and a stacked RSB system forms.

Whereas the basinward RSB is very similar to previous models of basinward-dipping ramps (Figs. 13 and 17), the geometry of the landward RSB is different when compared to the previous model of a RSB formed above a landward-dipping ramp. Because the landward RSB moves over the second, basinward-dipping step, it subsides and rotates further, thus, having a steeper, basinward dip (Fig. 17). This is seen in RSB 5 where the lower, landward RSB is steeper above the basinward-dipping ramp, being limited by a wide (>5 km) salt wall (Fig. 10).

5.5. Translation history and depocentre migration

To analyse the tri-dimensional kinematics and evolution of the RSBs mapped, we present true-stratigraphic thickness maps from one RSB (RSB 5, figs. 10 and 18). These maps have similar trends and shapes for each mapped interval; and consistent amount (1.8-3 km) and direction of offset (120 $\pm$ 15°) through time Fig. 18), which indicate they are formed in response to a single and relatively steady process, i.e. translation. The consistent offset towards the SE to ESE is roughly perpendicular to the main base-salt steps and parallel to the regional gravity-driven tectonic transport direction (Quirk et al 2012; Jackson et al 2014). The depo-thicks of all five RSBs presented in this study are located basinward or above base-salt ramps (Fig. 18).

By summing the offsets between the thickest points on each map of fig. 18, a total translation of 26.9 km was obtained. However, this measure does not represent the total translation of this basin as we do not present thickness maps for the first and last onlapping intervals. Due to limited seismic resolution and uncertainties related to salt-related faulting and folding (Fig. 10), it was not possible to generate accurate thickness maps of these intervals in none of the RSBs mapped. Nevertheless, it was possible to obtain confident estimates of translation within these systems by comparing thickness maps with multiple dip-oriented cross-sections (Figs. 7-10), where we measured the distance of the first onlap point to the top of the ramp, a methodology also used by Jackson and Hudec(2005).

RSB 5 demonstrates the larger amount of overall translation in the SPP, estimated as 32 km (Fig. 10 and 18). In many other examples, we were only able to determine a minimum translation because they are located at the eastern edge of the data, such as in RSB 1 (9.5 km of translation), RSB 2 (18 km) and RSB 4 (16 km); or are eroded or heavily deformed by diapirism. Nonetheless, less-deformed and less–eroded examples situated far from the edges of the data allowed more precise estimates of cover translation in the area, which vary from 28 km in the south (RSB 3, fig. 8) to 32 km to the north (RSB 5, fig. 11). Stacked RSBs were important to guarantee a higher degree of certainty in areas of complex salt deformation or intense erosion, because they record the same amount of translation (Jackson and Hudec, 2005) and, thus, can be used as a cross-check. As seen in RSB 5, both the landward and basinward RSBs present 32 km of translation (Fig. 11).

Using age constraints provided Modica and Brush, 2004; Guerra and Underhill, 2012; Jackson et al. 2015, it was possible to confirm the time of onset of translation as being Top-Albian; and to estimate the end of translation to vary from top-Cretaceous (Fig. 8) to mid-Paleocene (Fig. 7, 9 and 10). Although there is a small degree of uncertainty regarding these age estimates, we can obtain an approximate average translation rate of 0.7 – 0.9 mm/yr.

6. Discussion

6.1. Extensional vs. salt-related RSBs

Classical RSBs (Fig. 1a-b), are generated by regional extension, in which the controlling fault cuts progressively downwards through pre-kinematic strata. Consequently, this interval appears both above and below the fault. The basal boundary is, thus, defined by an extensional rollover composed of pre-kinematic strata and a fault surface that is formed at the onset of translation and maintain its original geometry through time (Fig. 1a-b). The pattern of vertical movement of the hangingwall is controlled by the shape of the extensional fault. As a consequence, the geometry and location of the subsiding minibasin does not change as the system evolves, and the rate of subsidence is directly proportional to the rate of lateral translation. Therefore, in an extensional RSB, translation of the cover can result in subsidence, but not in uplift (Fig. 1a-b).

In contrast, salt-detached RSBs are not directly driven by extension. Instead, they form by cover translation above salt (Fig. 1c-d), which, in turn, occurs in response to gravity-driven extension updip and is linked to contraction or salt advance downdip (Jackson and Hudec, 2005; Jackson et al 2015). The basal slip surface is stratabound, i.e. parallel to the pre-kinematic stratigraphy (Jackson and Hudec, 2005), so pre-kinematic strata always occur below their basal surface (Fig. 1c-d). The base-salt relief is usually related to inherited topography due to previous basement faulting; so translation and RSB development are decoupled from pre-salt deformation.

Movement takes place by shearing of a slip volume (viscous salt) rather than a discrete slip surface (extensional fault in classical RSBs) (Fig. 1c-d). Thus, salt drag, expulsion and diapirism generate vertical movements, additional accommodation and complexities not observed in extensional systems. The shape and size of the subsiding minibasin changes as the system evolves, because the geometry and thickness of the salt detachment vary as the cover moves. Additionally, as the RSB evolves with increasing displacement, vertical movement of the surface may change from laterally variable subsidence, to subsidence plus local uplift (Fig. 1c-d).

6.2. Kwanza vs. Santos Basin RSBs: thin vs. thick salt RSBs

In the Kwanza Basin, RSBs formed by 23-26 km of salt-detached translation over a major base-salt step (Atlantic Hinge Zone), in response to extension further updip (Fig. 19) (Peel et al. 1998, Hudec and Jackson, 2004, Jackson and Hudec, 2005; Peel 2014). These RSBs consist of a synclinal growth interval that dips and expands landward (E-ENE) towards a diachronous basal boundary that becomes younger and steeper landward (Fig. 19). They are defined by a basinward-dipping axial trace that also becomes steeper landward and their updip edge occurs immediately above a base-salt basinward-dipping ramp (Jackson and Hudec, 2005; Peel 2014). This geometry, stratigraphic architecture and relationship with base-salt topography are notably similar to the examples shown in the SPP, Santos Basin (Figs. 6-10).

However, RSBs in the SPP (Figs. 6-10) have a more complex stratigraphic architecture, with pronounced folding and rotation of syn-kinematic strata, when compared to similar systems in the Kwanza Basin (Fig. 19). This contrast is explained by the stronger effects of synchronous to late diapirism deforming and segmenting RSBs in the SPP, which, in turn, are related to the differences in salt thickness between the two basins (compare salt thickness between Figs. 3b and 19). In the Kwanza Basin, RSBs are present above a relatively thin (>1 km, Peel 2014), and, now exhausted/welded salt layer; and most of the diapirs were already developed prior to the onset of translation (Jackson and Hudec, 2005). Salt was already relatively thin at the onset of translation (Fig. 19a) and a combination of layer-parallel shearing and salt expulsion beneath the RSB lead to its dramatic thinning and welding over the ramp, and consequent inflation further basinward (Fig. 19b-c). This inhibited vertical salt movements and diapirism during translation and generation of RSBs.

Across the Atlantic, in the SPP, the RSBs are now present above thick (>2 km), layered salt and pre-translation salt structures are rare, with most diapirs forming during translation and development of RSBs (Figs. 6-10), i.e. post-Albian (Jackson et al. 2015). Despite the relatively large thickness of salt detachment, intra-salt layering favoured intra-salt layer-parallel shearing (i.e. Couette flow), which was accommodated in intra-salt detachment horizons and by seaward-vergent shear zones (Figs. 6-8). Sedimentation within RSBs above thick salt imposed an additional loading into the source-layer immediately beneath the RSB, expelling salt to its surroundings and promoting diapirism (Figs. 8-10), which become increasingly important through time as the overburden thickens (Jackson and Hudec, 2005). Thus, synchronous diapirism acted as a stronger second-order control in

RSB evolution in the SPP than in the Kwanza Basin, which resulted in higher degree of folding, rotation and localized erosion (Figs. 8-10), which can obliterate RSBs original geometries.

Another important contrast between these two basins regards the timing and rate of translation. In the Kwanza Basin, the RSBs are capped by the seafloor at their landward edges, which demonstrates ongoing activity (Fig. 19) (Jackson and Hudec, 2005). However, when translation started remains unclear (Jackson and Hudec, 2005). These authors estimate that translation over the Atlantic Hinge Zone and development of RSBs initiated in the mid Miocene. This would correspond to a total translation time of 12-13 Myr at a rate of 2 mm/year, which is surprisingly 2-4 times higher than typical deformation rates of salt-detached gravity-driven systems (Rowan et al. 2004).

In the SPP, however, translation and RSB generation started at the end of the Albian and stopped during the early- to mid Paleocene (Figs. 6-10). As translation varied from 28 km to 32 km, movement occurred at an approximate rate of 0.7 – 0.9 mm/year. These are relatively fast, but comparable to deformation rates measured in Gulf of Mexico (0.1 – 0. 5 mm/yr) and Kwanza Basin (0.4-0.5 mm/yr) (Rowan et al. 2000; 2004). Although, the amount and pattern of translation between the two basins is remarkably similar, the difference in timing and rate is thus considerable. We still do not fully understand these contrasts but we believe that, due to the nature of the 2D data and the limited well-control from the earlier work of Jackson and Hudec (2005), their estimate of when translation began in the Kwanza Basin may be inaccurate. A similar and more recent study from these authors (Dooley et al. 2017) shows one RSB from the Campos Basin, Brazil, where translation started at the end of the Albian as in the SPP, supporting our interpretation.

Why translation is still ongoing in the Kwanza Basin and stopped in the Santos Basin is out of the scope of this study, as this would require a more regional analysis involving transects comprising the whole extent of the salt basins in both margins. However, a few factors can explain why translation ceased in the SPP: 1) the mobile salt interval, i.e. halite, represented by the transparent seismic facies within the salt, thinned dramatically in between diapirs (Figs. 6-9), reducing mobility of the system; 2) dip reversal of the detachment due to the enormous sedimentary loading associated with the Albian Gap landward of the SPP (Fig.3) (Davison et al. 2012); and 3) the system reached the contractional domain as it is now located at the toe-of-slope (Fig.3b).

6.3. Occurrence of RSBs in other salt basins

There are currently very few publications describing salt-related RSBs. Apart from Rowan (2014) and Dooley et al. (2017), who briefly describe RSBs in the Red Sea and Campos Basin, respectively; all previous studies refer exclusively to RSBs in the Kwanza Basin, (Marton et al. 1998, Peel et al. 1998; Jackson and Hudec, 2005). The question that remains is; therefore, how widespread are salt-related RSBs?

We believe that because of their unique and complex stratigraphic architecture, the very limited literature about the subject, the lack of a detailed 3D analysis and modelling of these features, and because they are commonly affected by other salt tectonic processes, RSBs have been previously overlooked. As an example of their occurrence in other salt basins, we present a 2D seismic profile through a RSB formed above allochthonous salt in the Essaouira-Agadir Basin, offshore Morocco (Fig. 20).

In the western portion of the section, there is a clear example of a RSB formed above thick (~1 km) allochthonous salt with a basinward-dipping ramp at its base. The RSB is characterized by asymmetric and gently folded strata thickening and dipping mainly landward towards a diachronous basinward-dipping onlap surface. The system is defined by a steep basinward-dipping axial trace and onlap stratal terminations that grade upward into transitional boundaries (Fig. 12), a geometry characteristic of systems with relative high $\dot{A}/\dot{T}$. Total translation recorded is 9.4 km during Paleocene to Pliocene times, equivalent to rates of 0.15-0.2 mm/year, comparable with previous estimates of salt translation rates (Rowan et al. 2004).

The RSB is bounded updip by extensional domain with normal faults and an extensional rollover and downdip by an inflated salt tongue that was formed early by open-toe advance with late folding and uplift during the final stages of evolution of the RSB (Fig. 20). There is also another potential candidate for an RSB occurring further updip but the seismic data quality in this part of the section renders the interpretation of the updip RSB and its causal ramp somewhat speculative.

7. Conclusion

We mapped and presented detailed descriptions and thickness maps of salt-detached RSBs formed above thick (> 2 km) salt in the São Paulo Plateau, Santos Basin, Brazil. We compared our seismic interpretation to forward models simulating cover translation and viscous salt drag above variable base-salt topography to analyse the kinematics and sequential evolution of RSBs and, explain their geometries and relationship with base-salt topography.

In the SPP, RSBs show consistent magnitudes of total translation, varying from 28 to 32 km; and movement direction, which varies from ESE to SE. We have demonstrated that these systems have similar geometries, stratigraphic architecture and relationship to base-salt steps when compared to previously published examples from the Kwanza Basin (Jackson and Hudec, 2005, Peel 2014). However, in the SPP, ramp-syncline basins are generally more complex because they occur above thick salt and, consequently, are more affected by synchronous diapirism and salt-related deformation. We have also demonstrated that cover translation above landward-dipping ramps can generate notably similar stratal geometries to classical examples of RSBs formed above basinward-dipping ramps and that these systems exist in the south-central segment of the SPP.

As seen from seismic examples and models, there is a direct relationship between RSB evolution and base-salt topography, as RSBs finish updip above the top of base-salt ramps, or above diapirs formed over the ramp. Thus, mapping of RSBs can aid in the identification of pre-salt structures, being extremely useful in areas of limited data or limited sub-salt data quality when exploring for sub/pre-salt exploration targets. Ultimately, this study improves our current knowledge of RSBs, working as a guide for seismic interpretation and recognition of these systems in other salt basins around the world in the future.

8. Acknowledgements

We wish to thank Mike Hudec, Jonathan Redfern, Gillian Apps and Sian Evans for sharing their insights and criticisms. We thank CGG for providing access to the 3D seismic dataset used in this study as well as ONHYM for allowing us to use one seismic section offshore Morocco. The main author would also like to thank the Science without Borders program and CNPq, Brazil for sponsoring his PhD research. Schlumberger is also acknowledged for provision of Petrel software to the University of Manchester.

9. References

Alves, T. M., Fetter, M., Lima, C., Cartwright, J. A., Cosgrove, J., Gangá, A, & Strugale, M. (2017). An incomplete correlation between pre-salt topography, top reservoir erosion, and salt deformation in deep-water Santos Basin (SE Brazil). *Marine and Petroleum Geology*, *79*, 300-320.

Barton, N., 2007. Rock quality, seismic velocity, attenuation and anisotropy. CRC press.

Benedicto, A., Séguret, M., & Labaume, P. (1999). Interaction between faulting, drainage and sedimentation in extensional hanging-wall syncline basins: Example of the Oligocene Matelles basin (Gulf of Lion rifted margin, SE France). *Geological Society, London, Special Publications*, *156*(1), 81-108.

Carminatti, M., Wolff, B. & Gamboa, L. (2008). New exploratory frontiers in Brazil. In 19th World Petroleum Congress. World Petroleum Congress.

Contreras, J., Zühlke, R., Bowman, S., & Bechstädt, T. (2010). Seismic stratigraphy and subsidence analysis of the southern Brazilian margin (Campos, Santos and Pelotas basins). *Marine and Petroleum Geology*, *27*(9), 1952-1980.

Cobbold, P. R., Szatmari, P., Demercian, L. S., Coelho, D., & Rossello, E. A. (1995). Seismic and experimental evidence for thin-skinned horizontal shortening by convergent radial gliding on evaporites, deep-water Santos Basin, Brazil. *In:* Jackson, M. P. A., Roberts, D. G., Snelson, S. (eds) *Salt tectonics: a global perspective.* AAPG Memoir 65, 305-321.

Demercian, S., Szatmari, P., & Cobbold, P. R. (1993). Style and pattern of salt diapirs due to thin-skinned gravitational gliding, Campos and Santos basins, offshore Brazil. *Tectonophysics*, *228*(3-4), 393-433.

Duval, B., Cramez, C., & Jackson, M. P. A. (1992). Raft tectonics in the Kwanza basin, Angola. *Marine and Petroleum Geology*, *9*(4), 389-404.

Ellis, P. G., & McClay, K. R. (1988). Listric extensional fault systems-results of analogue model experiments. *Basin Research*, *1*(1), 55-70.

Davison, I., Anderson, L., & Nuttall, P. (2012). Salt deposition, loading and gravity drainage in the Campos and Santos salt basins. *Geological Society of London Special Publications*, *363*(1), 159-174.

Dooley, T. P., Jackson, M. P., Jackson, C. A. L., Hudec, M. R., & Rodriguez, C. R. (2015). Enigmatic structures within salt walls of the Santos Basin—Part 2: Mechanical explanation from physical modelling. *Journal of Structural Geology*, *75*, 163-187.

Dooley, T. P., Hudec, M. R., Carruthers, D., Jackson, M. P., & Luo, G. (2016). The effects of base-salt relief on salt flow and suprasalt deformation patterns—Part 1: Flow across simple steps in the base of salt. *Interpretation*, *5*(1), SD1-SD23.

Fiduk, J. C., & Rowan, M. G. (2012). Analysis of folding and deformation within layered evaporites in Blocks BM-S-8 &-9, Santos Basin, Brazil. *Geological Society, London, Special Publications*, *363*(1), 471-487.

Gibbs, A. D. (1984). Structural evolution of extensional basin margins. *Journal of the Geological Society*, *141*(4), 609-620.

Guerra, M. C., & Underhill, J. R. (2012). Role of halokinesis in controlling structural styles and sediment dispersal in the Santos Basin, offshore Brazil. *Geological Society, London, Special Publications*, *363*(1), 175-206.

Flinch, J., 2014. Context, challenges, and future of deep-water plays: an overview. Search and Discovery Article, 41417.

Gomes, P.O., Kilsdonk, B., Grow, T., Minken, J. & Barragan, R. (2012). Tectonic evolution of the outer high of Santos basin, southern Sao Paulo Plateau, Brazil, and implications for hydrocarbon exploration. *In*: Gao, D. (eds) *Tectonics and Sedimentation: Implications for Petroleum Systems*. AAPG Memoir 100, 125–142.

Hudec, M. R. & Jackson, M. P. A. (2004). Regional restoration across the Kwanza Basin, Angola: Salt tectonics triggered by repeated uplift of a metastable passive margin. *AAPG bulletin*, *88*(7), 971-990.

Jackson, M. P. A. & Cramez, C. (1989). Seismic recognition of salt welds in salt tectonics regimes. *In: Gulf of Mexico salt tectonics, associated processes and exploration potential: Gulf Coast Section SEPM Foundation 10th Annual Research Conference*, 66-71.

Jackson, M. P. A., Hudec, M. R., Fraenkl, R., Sikkema, W., Binga, L. & Da Silva, J. (2001). Minibasins translating down a basement ramp in the deepwater monocline province of the Kwanza Basin, Angola [abs.]. *In*: *American Association of Petroleum Geologists Annual Meeting Official Program*, *10*, A99.

Jackson, M.P. & Hudec, M.R. (2017). Salt Tectonics: Principles and Practice. Cambridge University Press.

Jackson, M. P., & Hudec, M. R. (2005). Stratigraphic record of translation down ramps in a passive-margin salt detachment. *Journal of Structural Geology*, *27*(5), 889-911.

Jackson, C. A. L., Jackson, M. P., & Hudec, M. R. (2015). Understanding the kinematics of salt-bearing passive margins: A critical test of competing hypotheses for the origin of the Albian Gap, Santos Basin, offshore Brazil. *Geological Society of America Bulletin*, *127*(11-12), 1730-1751.

Jackson, C. A. L., Rodriguez, C. R., Rotevatn, A., & Bell, R. E. (2014). Geological and geophysical expression of a primary salt weld: An example from the Santos Basin, Brazil. *Interpretation*, *2*(4), SM77-SM89.

Jackson, C. A. L., Jackson, M. P., Hudec, M. R., & Rodriguez, C. R. (2015). Enigmatic structures within salt walls of the Santos Basin—Part 1: Geometry and kinematics from 3D seismic reflection and well data. *Journal of Structural Geology*, *75*, 135-162.

Jones, I. F., & Davison, I. (2014). Seismic imaging in and around salt bodies. *Interpretation*, *2*(4), SL1-SL20.

Karner, G. D., & Gambôa, L. A. P. (2007). Timing and origin of the South Atlantic pre-salt sag basins and their capping evaporites. *Geological Society, London, Special Publications*, *285*(1), 15-35.

Marton, G., Tari, G. & Lehmann, C. (1998) Evolution of salt-related structures and their impact on the post-salt petroleum systems of the Lower Congo Basin, offshore Angola. *In*: American Association of Petroleum Geologists International Conference and Exhibition, Rio de Janeiro. Extended Abstracts Volume, 834–834.

Marton, G., Tari, G. & Lehmann, C. (2000). Evolution of the Angolan Passive Margin, West Africa, With Emphasis on Post-Salt Structural Styles. *Atlantic rifts and continental margins*, 129-149.

McClay, K. R. (1990). Extensional fault systems in sedimentary basins: a review of analogue model studies. *Marine and petroleum Geology*, *7*(3), 206-233.

McClay, K. R., & Scott, A. D. (1991). Experimental models of hangingwall deformation in ramp-flat listric extensional fault systems. *Tectonophysics*, *188*(1-2), 85-96.

McClay, K. R. (1996). Recent advances in analogue modelling: uses in section interpretation and validation. *Geological Society, London, Special Publications*, *99*(1), 201-225.

771 Meisling, K. E., Cobbold, P. R., & Mount, V. S. (2001). Segmentation of an obliquely rifted margin, Campos and Santos basins, southeastern Brazil. *AAPG bulletin*, *85*(11), 1903-1924.

774 Modica, C. J., & Brush, E. R. (2004). Postrift sequence stratigraphy, paleogeography, and fill history of the deep-water Santos Basin, offshore southeast Brazil. *AAPG bulletin*, *88*(7), 923-945.

777 Mohriak, W.U., Macedo, J.M., Castellani, R.T., Rangel, H.D., Barros, A.Z.N., Latgé, M.A.L., Mizusaki, A.M.P., Szatmari, P., Demercian, L.S., Rizzo, J.G. & Aires, J.R. (1995). Salt tectonics and structural styles in the deep-water province of the Cabo Frio region, Rio de Janeiro, Brazil. *In:* Jackson, M. P. A., Roberts, D. G., Snelson, S. (eds) *Salt tectonics: a global perspective.* AAPG Memoir 65, 273-304.

782 Mohriak, W., Nemčok, M., & Enciso, G. (2008). South Atlantic divergent margin evolution: rift-border uplift and salt tectonics in the basins of SE Brazil. *Geological Society, London, Special Publications*, *294*(1), 365-398.

785 Mohriak, W., Szatmari, P., & Anjos, S. M. C. (2009). Sal: Geologia e Tectônica; Exemplos nas Bacias Brasileiras. *Terrae Didatica*, *4*(1).

787 Mohriak, W. U., Szatmari, P., & Anjos, S. (2012). Salt: geology and tectonics of selected Brazilian basins in their global context. *Geological Society, London, Special Publications*, *363*(1), 131-158.

790 Mohriak, W. (2015). Pre-Salt Carbonate Reservoirs in the South Atlantic and World-wide Analogs. In AAPG Geosciences Technology Workshop “Carbonate Plays around the World-Analogues to Support Exploration and Development (pp. 4-5).

793 Osmundsen, P. T., Bakke, B., Svendby, A. K., & Andersen, T. B. (2000). Architecture of the Middle Devonian Kvamshesten Group, western Norway: sedimentary response to deformation above a ramp-flat extensional fault. *Geological Society, London, Special Publications*, *180*(1), 503-535.

797 Peel, F., Jackson, M.P. & Ormerod, D. (1998) Influence of Major Steps in the Base of Salt on the Structural Style of Overlying Thin-skinned Structures in Deep Water Angola, American Association of Petroleum Geologists International Conference and Exhibition, Rio de Janeiro, Brazil, November, Extended Abstracts Volume, pp. 366-367.

801 Quirk, D. G., Schødt, N., Lassen, B., Ings, S. J., Hsu, D., Hirsch, K. K., & Von Nicolai, C. (2012). Salt tectonics on passive margins: examples from Santos, Campos and Kwanza basins. *Geological Society, London, Special Publications*, *363*(1), 207-244.

804 Peel, F. J. (2014). The engines of gravity-driven movement on passive margins: Quantifying the relative contribution of spreading vs. gravity sliding mechanisms. *Tectonophysics*, *633*, 126-142.

807 Rowan, M. G., Jackson, M. P., & Trudgill, B. D. (1999). Salt-related fault families and fault welds in the northern Gulf of Mexico. *AAPG bulletin*, *83*(9), 1454-1484.

809 Rowan, M. G., Peel, F. J., & Vendeville, B. C. (2004). Gravity-driven fold belts on passive margins.

811 Rowan, M. G., 2004, Do salt welds seal?: Presented at GCSSEPM Foundation 24th Annual Bob F. Perkins Research Conference, 390–403.

813 Rowan, M.G., 2014. Passive-margin salt basins: hyperextension, evaporite deposition, and salt tectonics. *Basin Research*, *26*(1), 154-182.

Sanchis, E. & Séranne, M. (2000). Structural style and tectonic evolution of a polyphase extensional basin of the Gulf of Lion passive margin: the Tertiary Ales basin, southern France. *Tectonophysics*, *322*(3), 219-242.

Schuster, D. C. (1995). Deformation of allochthonous salt and evolution of related salt-structural systems, eastern Louisiana Gulf Coast. *In:* Jackson, M. P. A., Roberts, D. G., Snelson, S. (eds) *Salt tectonics: a global perspective.* AAPG Memoir 65, 177-198.

Tari, G., & Jabour, H. (2013). Salt tectonics along the Atlantic margin of Morocco. *Geological Society, London, Special Publications*, *369*(1), 337-353.

Weijermars, R., Jackson, M. T., & Vendeville, B. (1993). Rheological and tectonic modeling of salt provinces. *Tectonophysics*, *217*(1-2), 143-174.

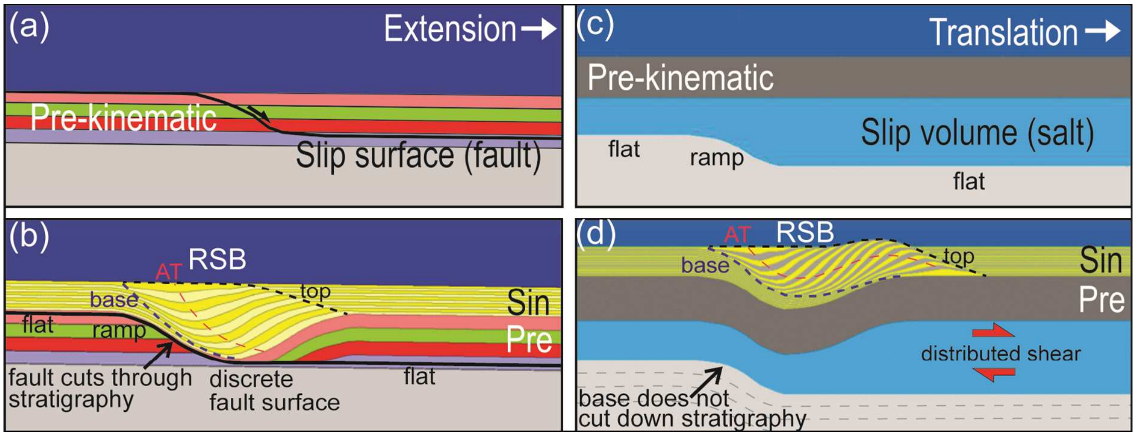

Figure 1: Models of RSB development. (a-b) represent "classic" RSBs, with (a) illustrating the system prior to deformation, and (b), the system during extension with development of a RSB characterized by an asymmetric depocentre with basinward-dipping axial trace (AT) above a discrete extensional fault that cuts down through stratigraphy in a ramp-flat trajectory. Movement of the hanging-wall creates differential amounts of subsidence and as long as the fault is extensional, there is no hanging-wall uplift. This contrasts with the model for salt-detached RSBs shown in (c-d). The system is not extensional; instead it the RSB forms by translation of the cover over a viscous salt layer. A downward offset of the base of salt takes the place of the fault ramp. The offset may not cut down through stratigraphy. Shear strain is distributed through the viscous salt and results in uplift on the downdip side of salt-detached RSBs. The base and top boundaries of the RSBs are diachronous, and consist either of onlap/offlap unconformity surfaces, or regions of abrupt stratal thinning.

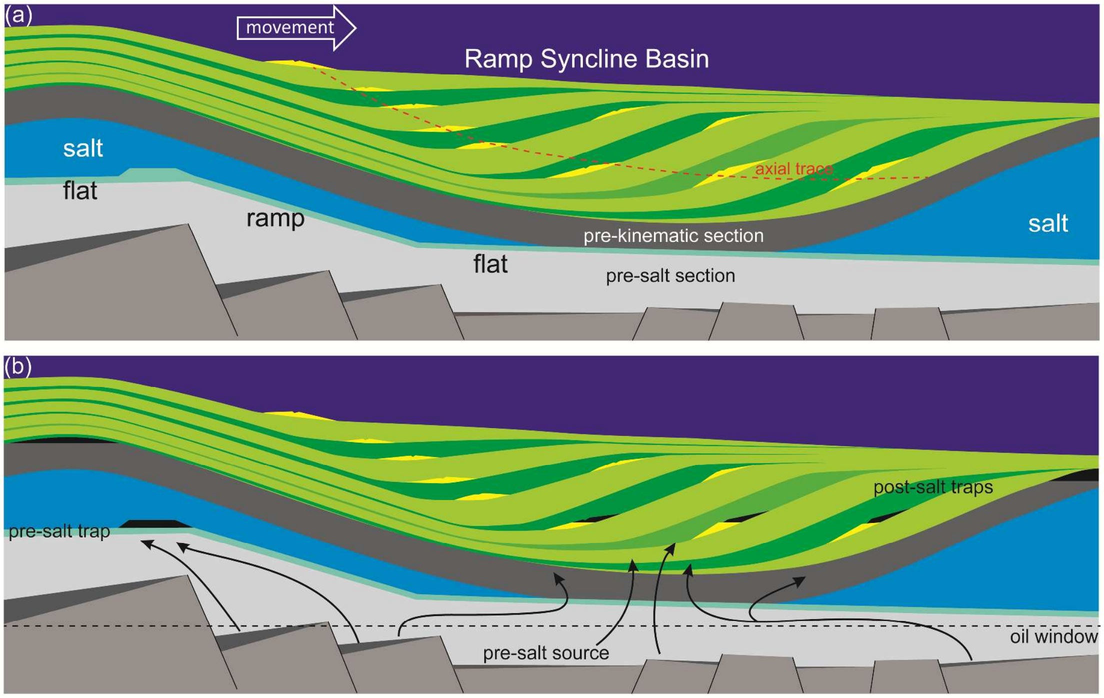

Figure 2: Schematic cross-sections: (a) illustrating typical geometry of RSBs formed above salt-detachments with a basinward-dipping ramp; and (b) displaying potential hydrocarbon plays that can be associated with RSBs in these settings: pre-salt carbonates (blueish green) occurring at the top of the pre-salt ramps and below the updip limit of the RSBs (e.g. Tupi and Iracema discoveries); carbonates on the crest of salt anticlines, and supra-salt sandier intervals juxtaposed above deeper and mature pre-salt source rocks, which can be charged with salt welding below the RSB.

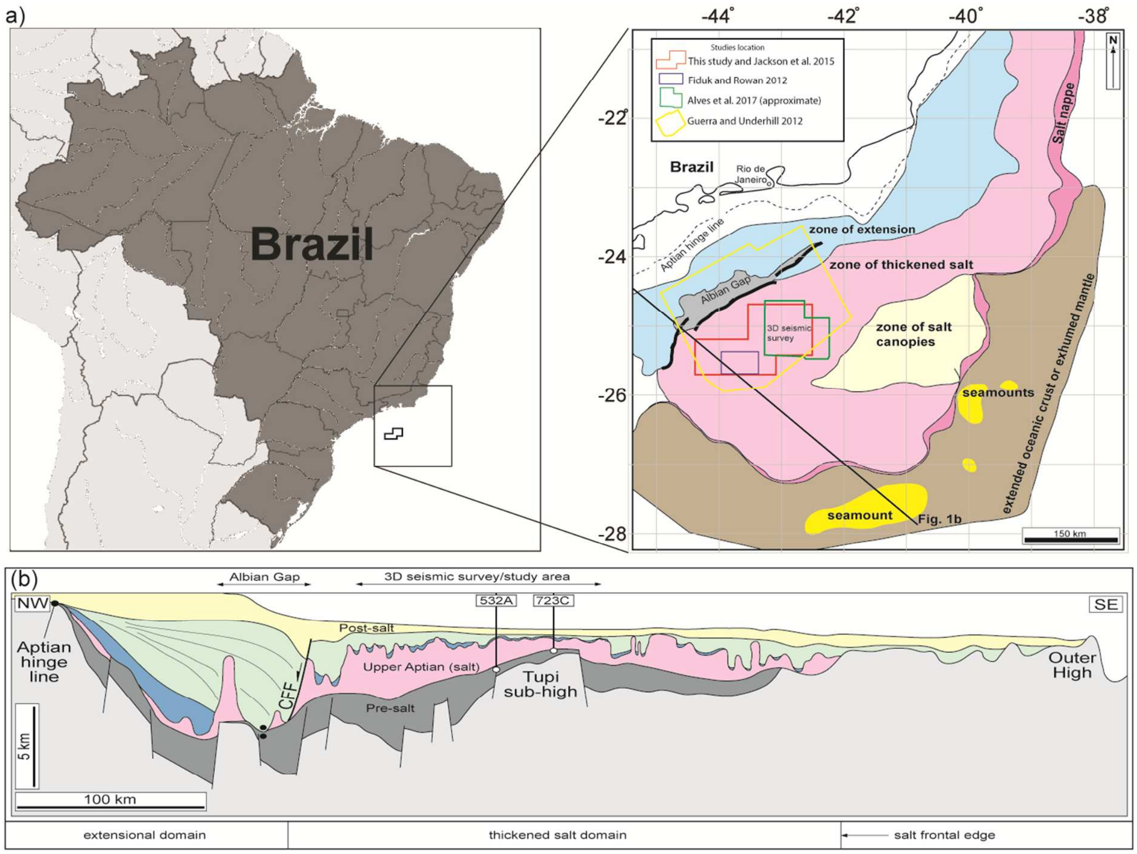

Figure 3: (a) Location map showing the 3D dataset and study area (Jackson et al. 2015) in its regional context. (b) Simplified geoseismic section across the central Santos Basin illustrating basement structures and salt-related structural provinces. Location of section is shown in (a).

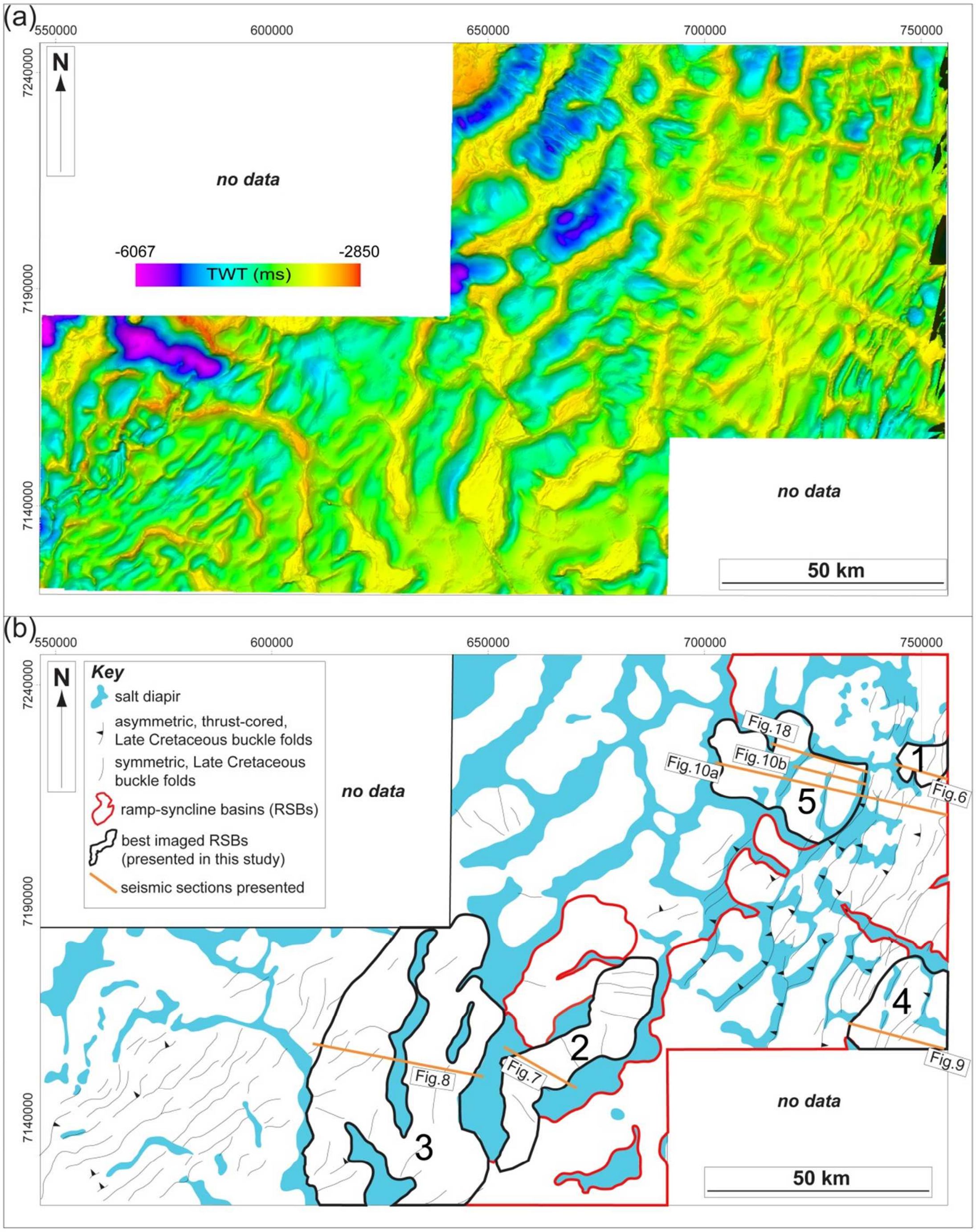

Figure 4: (a) Top-salt map showing complex pattern of salt walls and stocks. (b) Drawn top-salt map with main structures (adapted from Jackson et al. 2015), and distribution of RSBs. The examples presented in this study are in black polygons (RSB 1-5).

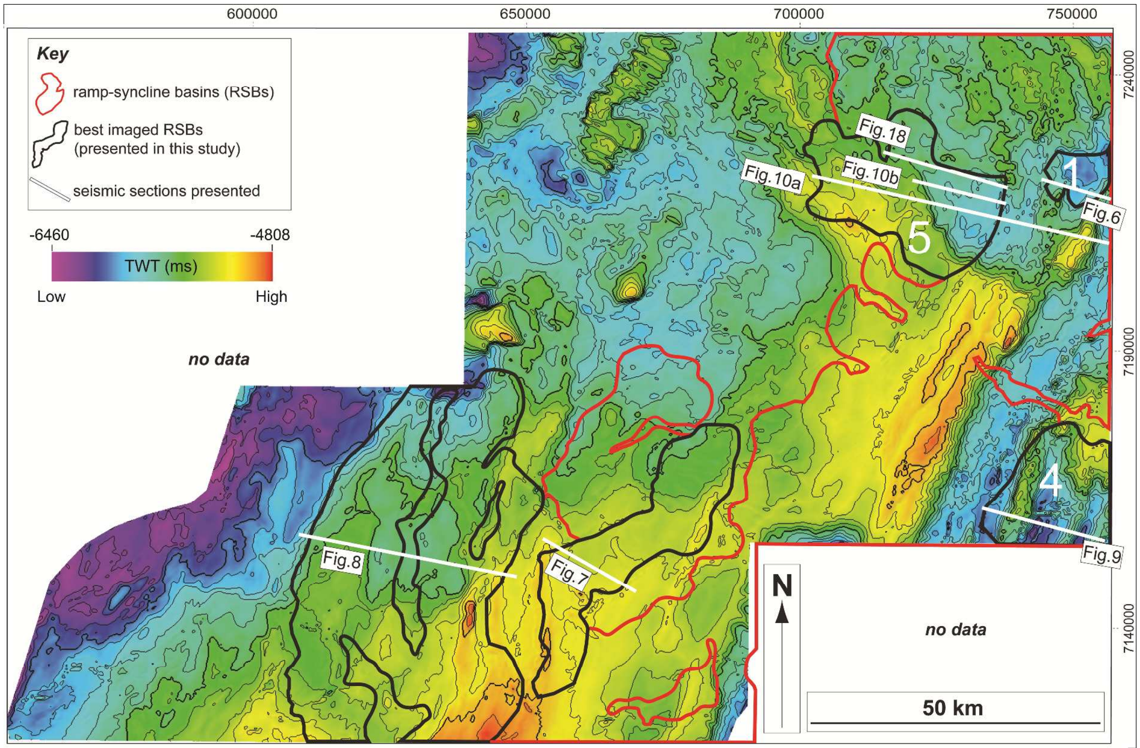

Figure 5: Static-corrected base-salt map showing the largest base-salt structures in the area. They trend NNE to NE, although the northernmost high (beneath RSB 5) trends NNW. Map shows that RSBs (red and black polygons) are distributed above and/or basinward of the main base-salt steps.

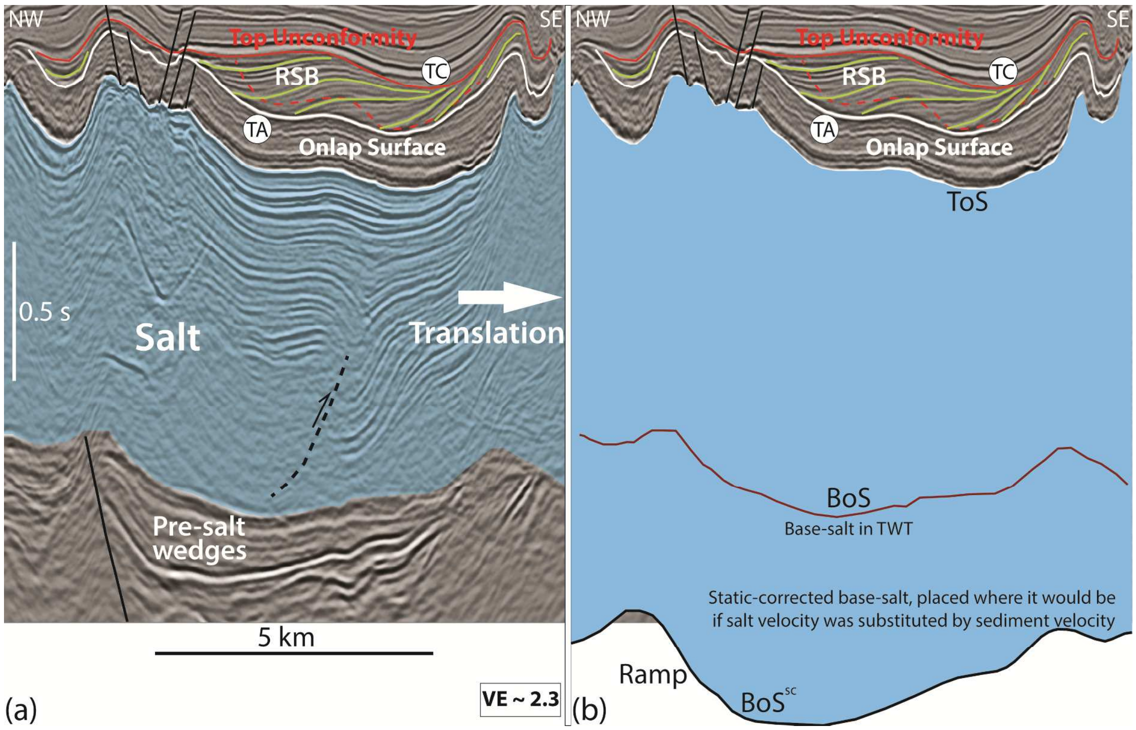

Figure 6: (a) Interpreted seismic section of RSB 1 with salt in blue and faults in black. Top Albian (TA) and top Cretaceous (TC) horizons based on Jackson et al. 2015. RSB characterized by landward-dipping and thickening sigmoidal strata (green) above an onlap surface (white, top Albian) and capped by a diachronous unconformity (red) that finishes updip at top Cretaceous. RSB axial trace (dashed red) steepens landward. Intra-salt seaward-vergent shear zones (black dashed lines) indicate lateral movement. Pre-salt wedges and faults are used as a cross-check of the static-corrected base-salt map and base-salt structures. In (b), the relationship between the RSB and base-salt structure is presented through the static-corrected base-salt (BoS^{sc}) which shows that the RSB landward edge occurs above the top of a base-salt basinward-dipping ramp.

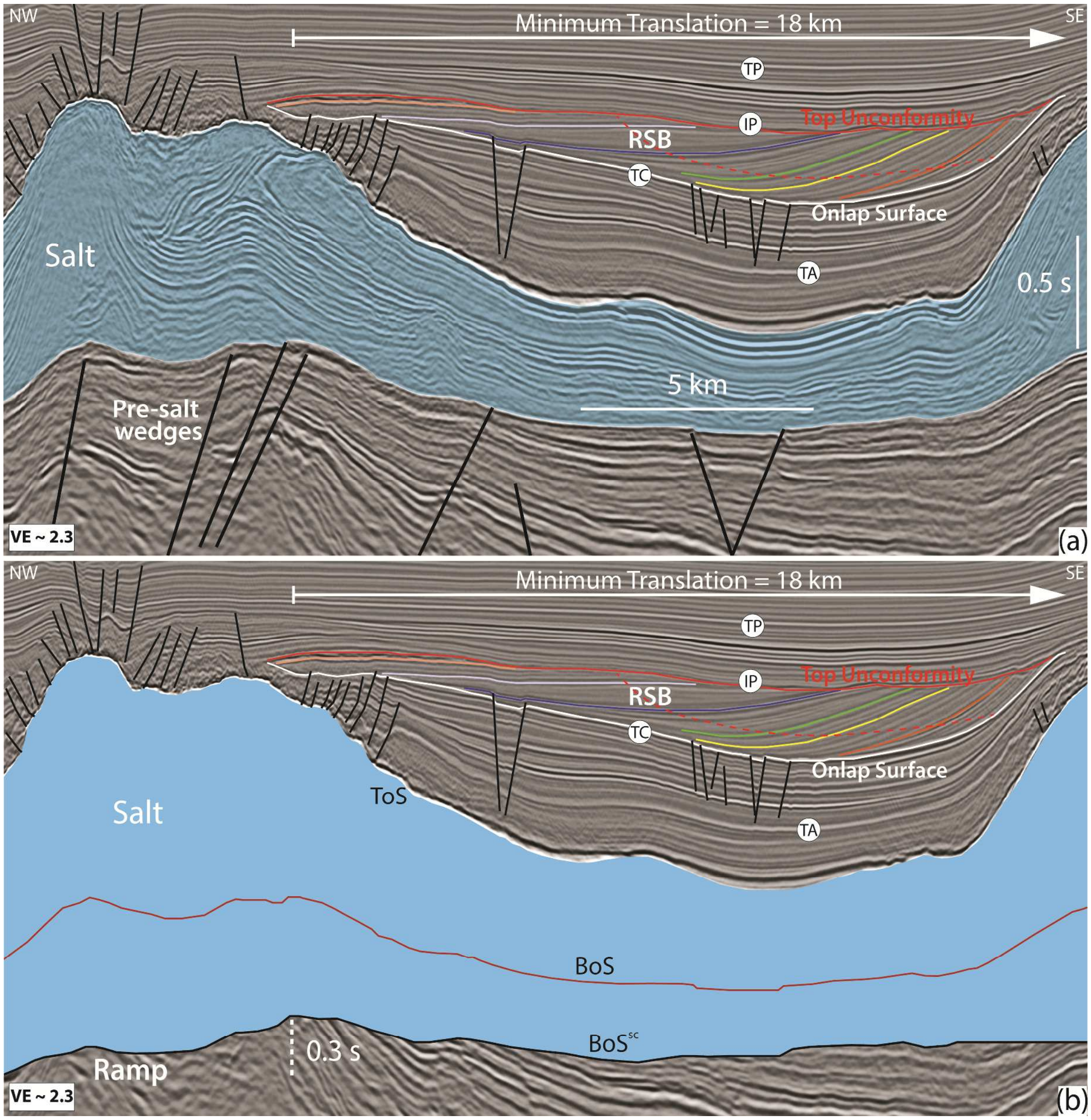

Figure 7: Seismic sections of the landward segment of RSB 2. Key horizons based on Jackson et al. 2015 are presented: top Albian (TA), top Cretaceous (TC), intra-Paleocene unconformity (IP) and top Paleocene (TP). In (a), interpretation of RSB 2, characterized by a well-defined onlap surface (white, TC) being onlapped by landward-dipping and thickening strata (colored lines), defined by a landward-steepening axial-trace (dashed red) and capped by the intra-Paleocene unconformity (red). Faults are in black. Pre-salt wedges and faults are used as a cross-check of static-corrected base-salt map and base-salt structures. In (b), the RSB is presented in the context of the static-corrected base-salt (BoS^{sc}) to illustrate that the RSB finishes updip above a base-salt landward-dipping ramp, being surrounded by diapirs. Minimum translation of 18 km is measured from first landward onlap point within the RSB to the top of the ramp.

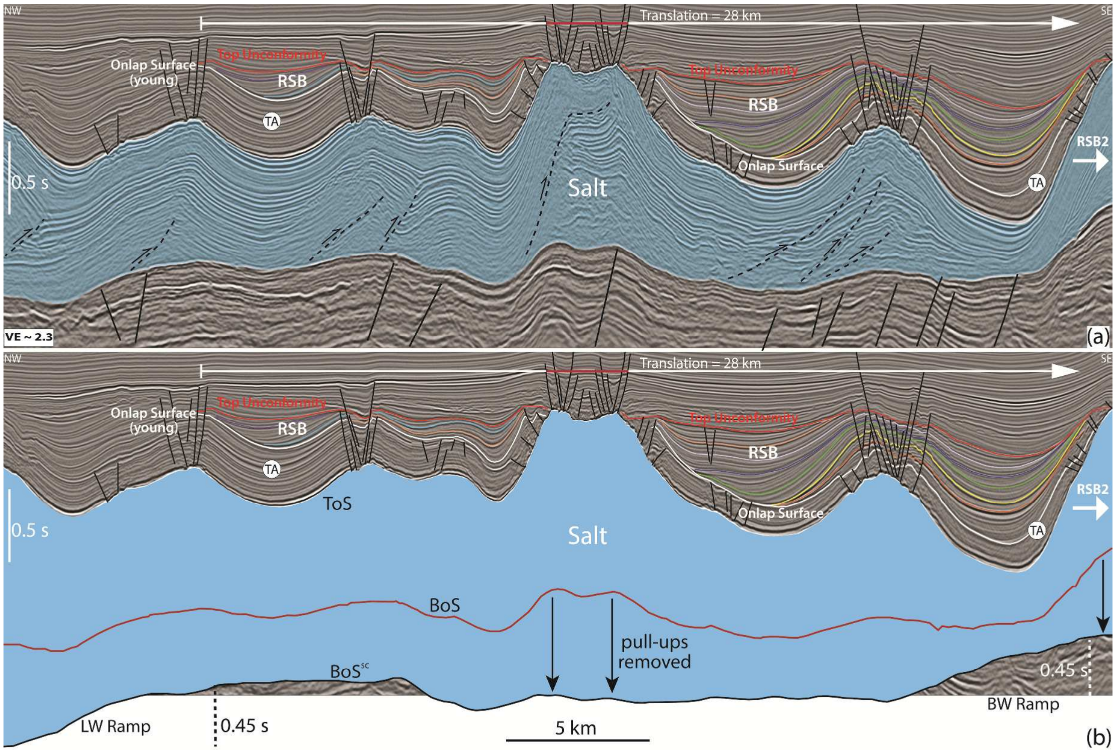

Figure 8: (a) Interpreted seismic section of the entire RSB 3 system showing a total of 28 km of translation. In (b), RSB is displayed in combination with the static-corrected base-salt (BoS^{sc}) to demonstrate its relationship with base-salt topography and how this approach eliminates velocity artefacts due to high velocities of the salt interval. The RSB is characterized by a well-defined and diachronous onlap surface (white) being onlapped by landward-dipping and thickening strata (colored lines) and truncated at the top by a diachronous unconformity (red). The basal onlap surface starts at the top Albian (TA) horizon and becomes progressively younger landward. RSB 3 is limited updip by a salt anticline formed above a landward-dipping base-salt ramp, and downdip by a large salt wall that also limits RSB 2 basinward. RSB 3 is segmented and folded by syn- to late diapirism. Faults are in black and pre-salt faults are used as a cross-check of base-salt structures. Intra-salt shear zones (black dashed lines) indicate lateral movement.

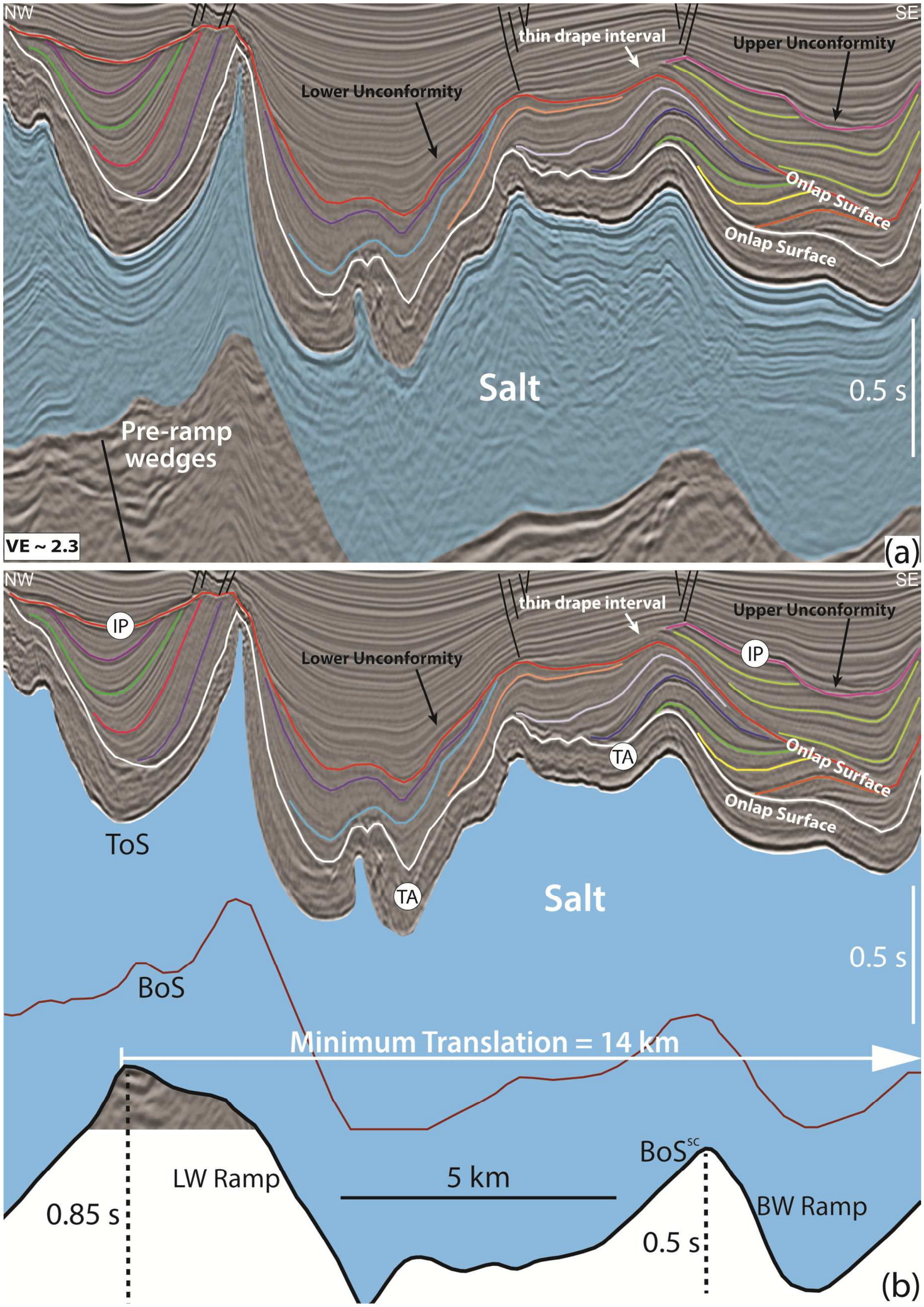

Figure 9: (a) Interpreted section of RSB 4 showing stacked RSBs and onlap surfaces (white and red). In (b) the stacked RSBs are show in the context of static-corrected base-salt (BoS^{sc}) and key horizons are presented: top Albian (TA), and intra-Paleocene unconformity (IP). Salt is in blue, faults in black and intra-RSB horizons in coloured lines. Onlap surfaces and top unconformity get slightly younger landward. Top unconformity of lower RSB corresponds to the onlap surface of upper RSB (red) until

becoming separated landward by a thin drape interval that is deposited updip of the basinward (BW) base-salt ramp and RSB. This surface (red) is aged mid-Cretaceous basinward and Intra-Paleocene landward evidencing its diachroneity. Only a minimum translation estimate of 14 km is obtained because RSB 5 is located at the edge of the data and is not visualized entirely.

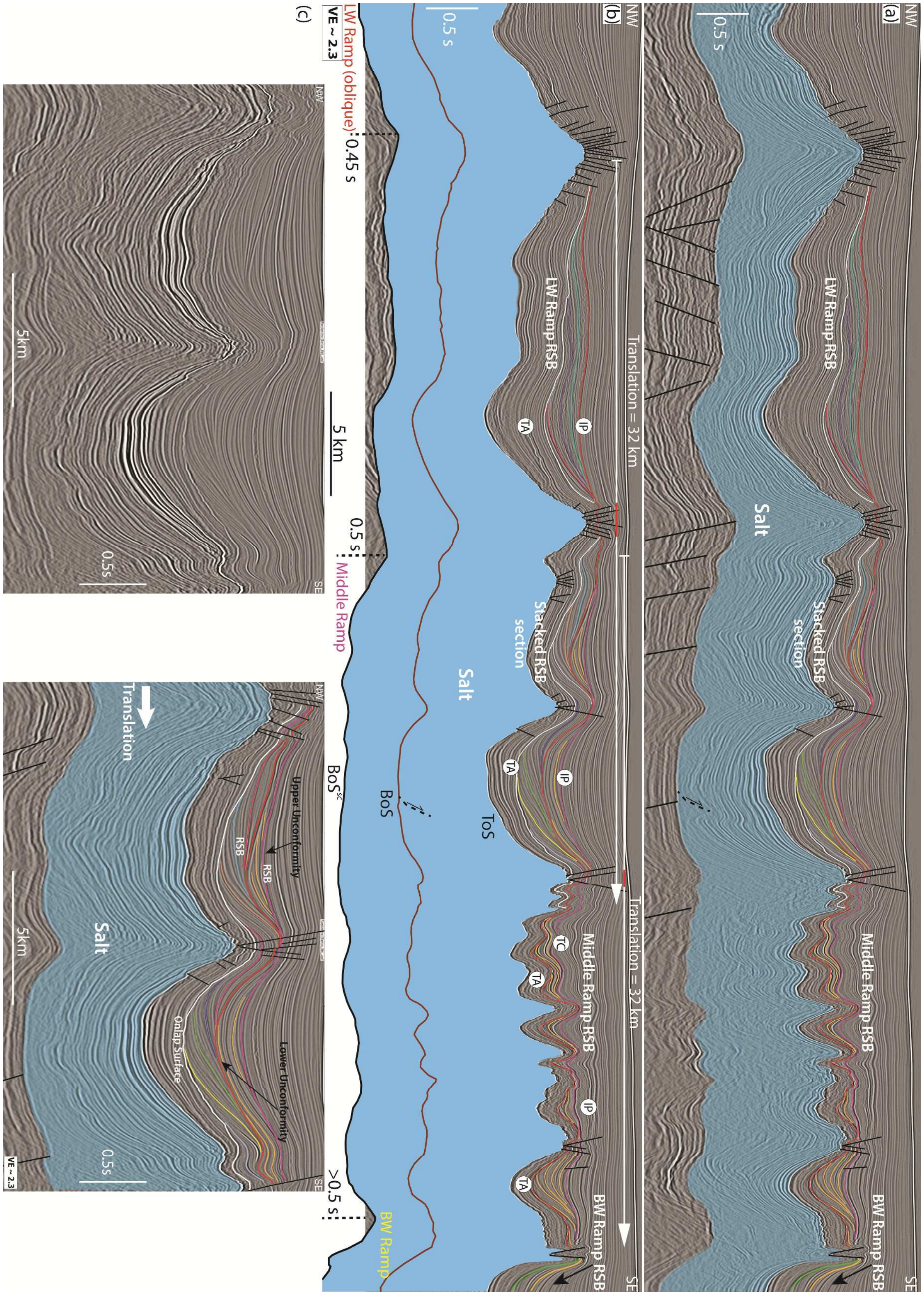

Figure 10: (a-b) Regional seismic sections of RSB 5 showing stacked RSBs and onlap surfaces (white and red lines) in the middle of the section. Salt is in blue and faults in black. In (b), the static-corrected base-salt (BoS^{sc}) and key horizons, top Albian (TA), top Cretaceous (TC) and intra-Paleoecene unconformity (IP) are presented. Three RSBs are shown: The basinwardmost one is

formed above a basinward-dipping ramp but appears only at the edge of the data. The middle RSB is formed by translation above a basinward-dipping ramp (middle ramp) and its landward portion is stacked on top of the basinward portion of the third, landward RSB, which is formed above a landward-dipping ramp. These RSBs are strongly affected by synchronous diapirism, folding and faulting but still show the typical geometries of RSB systems with sigmoidal landward-dipping and expanding strata. In (c), uninterpreted and interpreted localized sections of RSB 5, showing a zoom of the stacked RSBs section. A total of 32 km of translation is estimated for each of the stacked RSBs. The fact that both RSBs record the same amount of translation can be used as a cross-check for this measure.

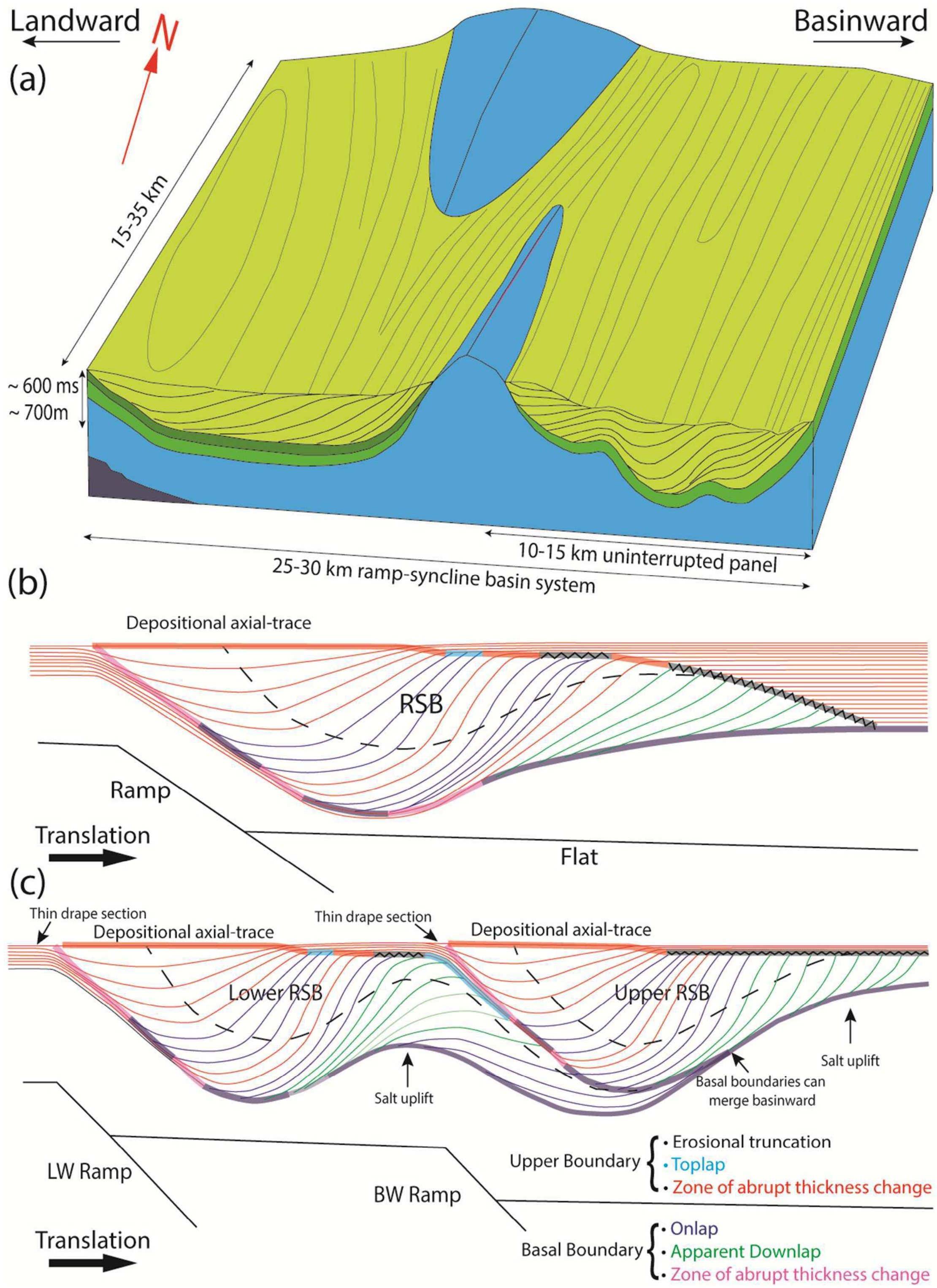

Figure 11: (a) Schematic 3D diagram of RSBs geometries, dimensions and relationship with diapirs and base-salt steps. (b) Summary of the 2D stratigraphic architecture showing the typical variations of strata termination of RSBs in the Santos Basin. The basal surface has terminations ranging from: i) abrupt apparent downlap at basinward edge, ii) abrupt onlap and iii) transition from thicker and steeper section within the RSB to a thin draping interval at its landward edge. The top unconformity

has a similar pattern of terminations ranging from abrupt erosional and toplap terminations downdip, to more transitional strata geometries updip. In (c), summary of the 2D stratigraphic architecture and strata terminations of stacked RSBs. The lower RSB finishes landward above the top of the landward ramp and the upper RSB finishes above the top of the basinward ramp. Stratal termination is similar to simple RSBs, but the lower RSB top unconformity acts as the onlap surface of the upper RSB along most of its length. A thin drape section can separate these surfaces at the upper RSB landward edge.

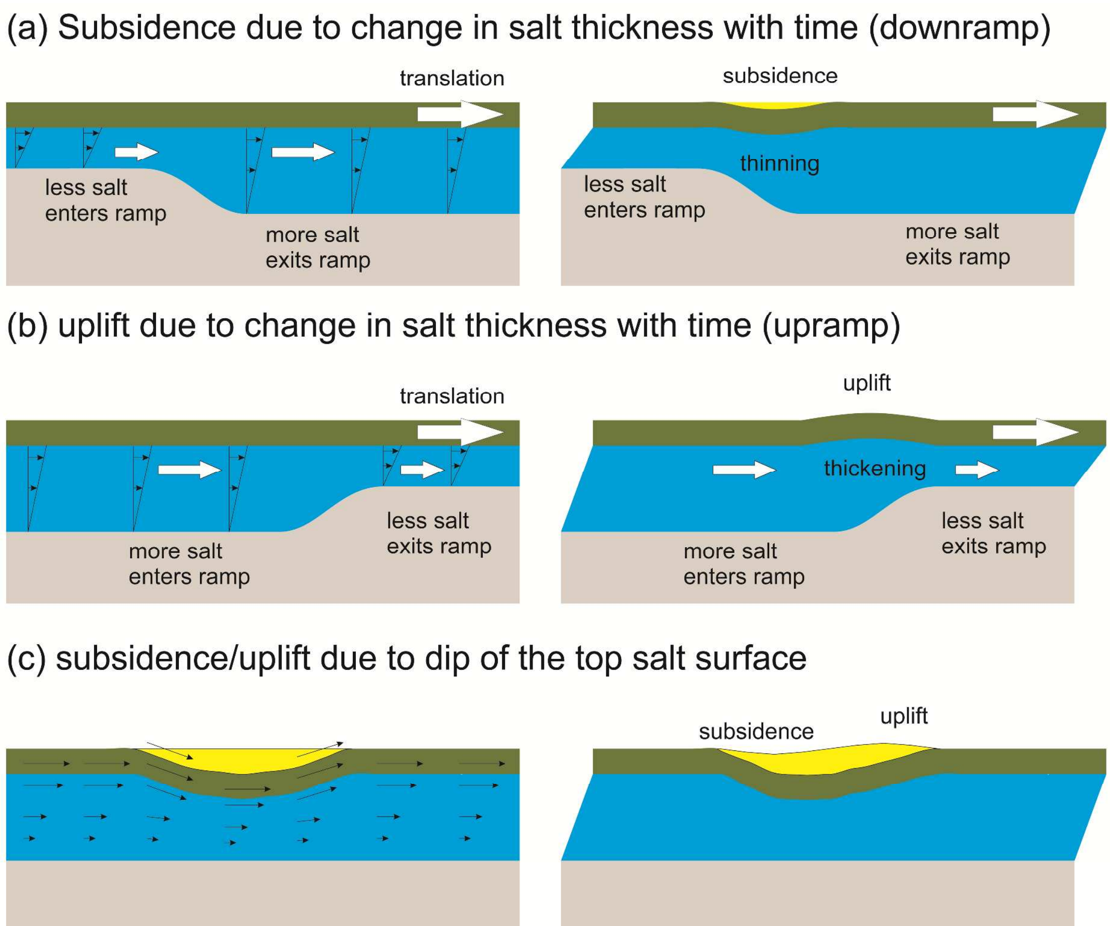

Figure 12: Conceptual 2D diagrams of the dynamics of Couette salt flow and variation of total salt-flux over a base-salt (a) basinward-dipping ramp and (b) landward-dipping ramp. In (a) the amount of salt leaving the ramp is lesser than the amount of salt arriving at the top of the ramp generating thinning of the salt layer, subsidence of the cover and generation of a depocentre immediately above the ramp. In (b), the amount of salt leaving the ramp is less than the amount of salt arriving, which results in salt thickening and uplift of the cover above the ramp. In (c), the diagram illustrates the effect of topography generated by translation above base-salt ramps by downward movement of the cover where the top-salt dips basinward and upward movement of the cover where the top-salt interval dips landward generating areas of local subsidence updip and uplift downdip.

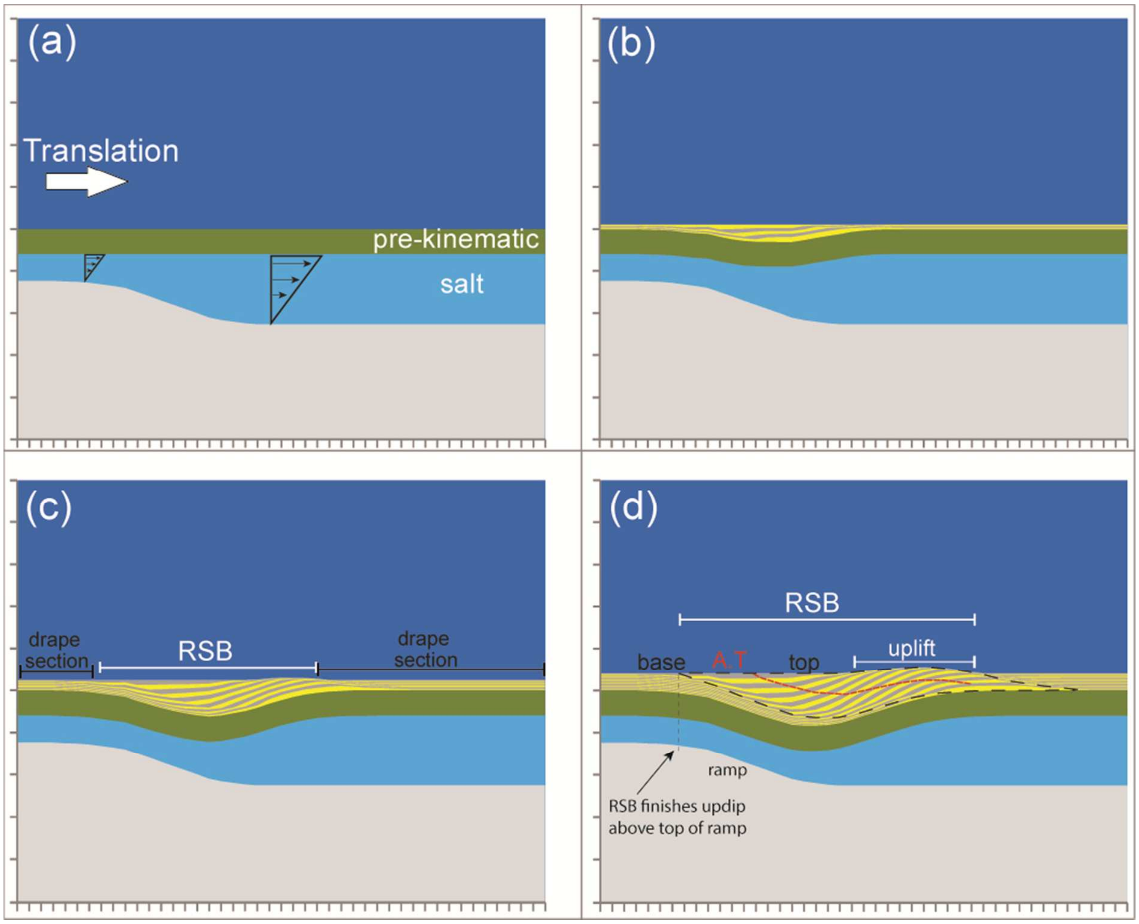

Figure 13: Numerical model simulating planar Couette flow and salt drag with overburden translation above a salt layer with a basal basinward-dipping ramp, which results in the development of a RSB above the ramp. Sequential evolution presented from (a) to (d). Syn-kinematic sediments are represented by yellow and grey layers.

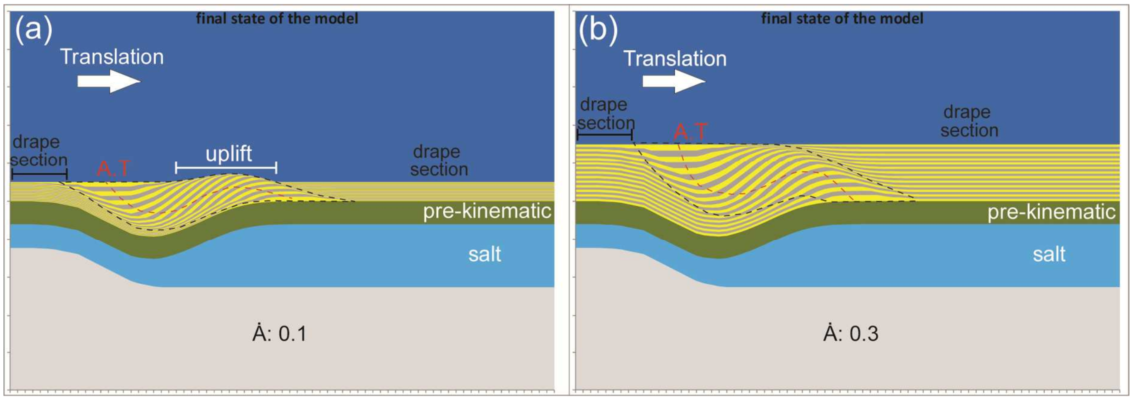

Figure 14: Final state of models simulating cover translation above a salt detachment with a base-salt ramp illustrating how variations of aggradation rate (Ȧ) can produce different stratigraphic architectures and stratal termination patterns. (Ȧ) in these models is non-dimensional so their variations are purely relative to translation rates (Ṫ). In (a) aggradation rate is 0.1 and the RSB is characterized by well-defined boundaries and uplift above the regional datum on the downdip side of the RSB. In (b) aggradation rate is 0.3 and the RSB is less asymmetric with upper and lower boundaries defined by a transition from thin section at regional dip to thicker and steeper section within the RSB. Translation rate (Ṫ) is the same in both models.

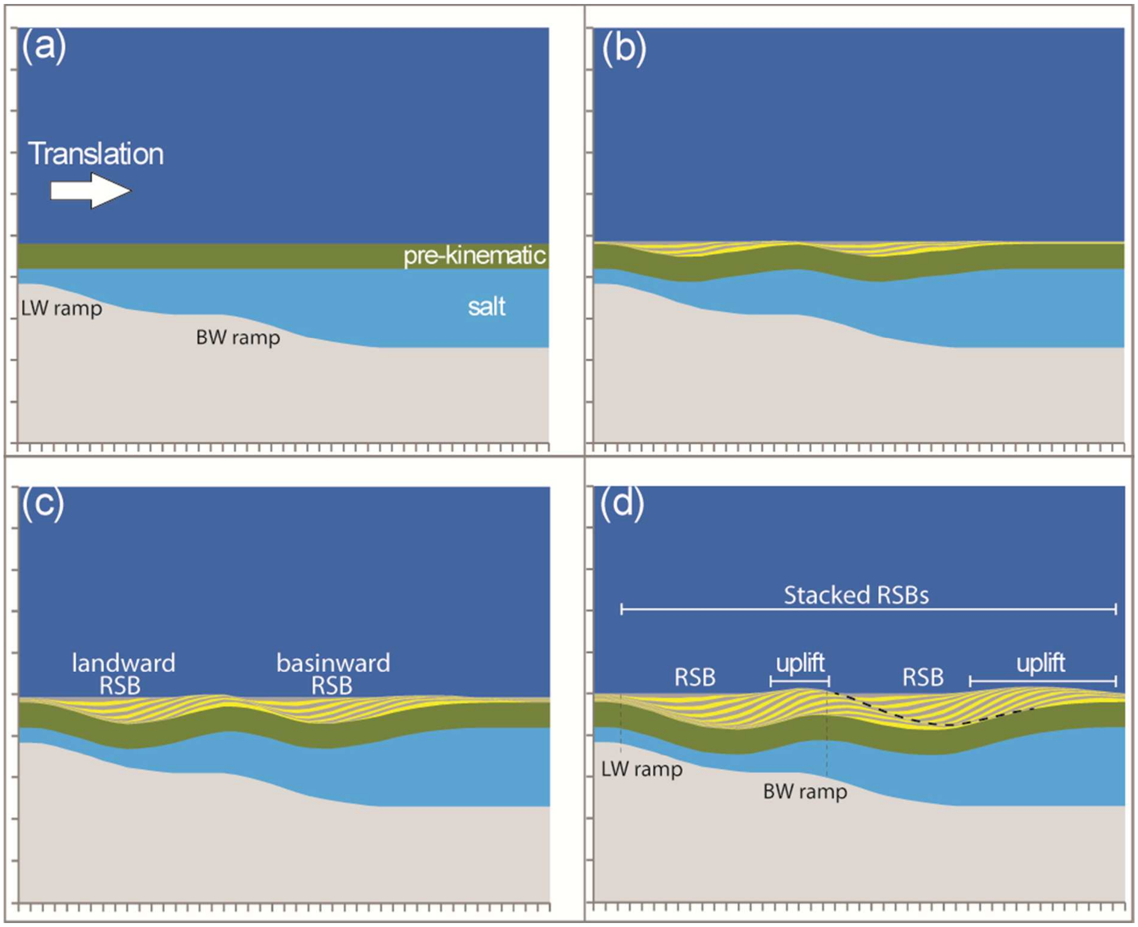

Figure 15: Numerical model simulating cover translation above a thick salt layer with 2 closely-spaced basinward-dipping ramps showing the sequential evolution of 2 stacked RSBs (a-d). The lower, landward RSB forms above the landward ramp while the upper, basinward RSB forms above the basinward ramp. Each of the RSBs finishes landward above their respective ramps. The top unconformity of the lower RSB acts as the onlap surface of the upper RSB (black dashed line). The upper and lower basal boundaries merge basinward while both top unconformities merge landward.

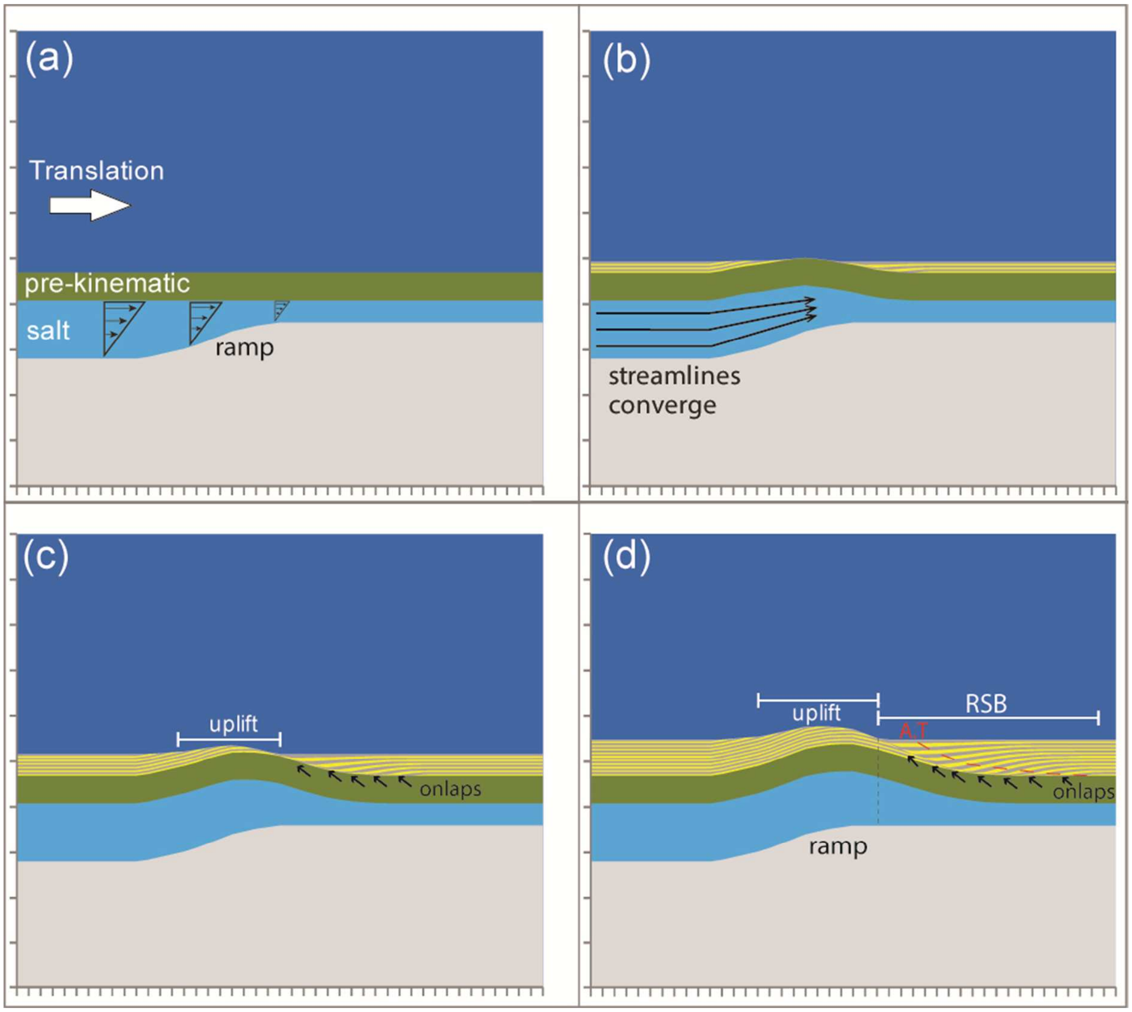

Figure 16: Numerical model simulating overburden translation and Couette salt flow above a landward-dipping base-salt ramp. Variations of salt flux across the step result in salt thickening over the ramp and development of a RSB basinward of it, above a base-salt flat. Sequential evolution is shown from (a) to (d).

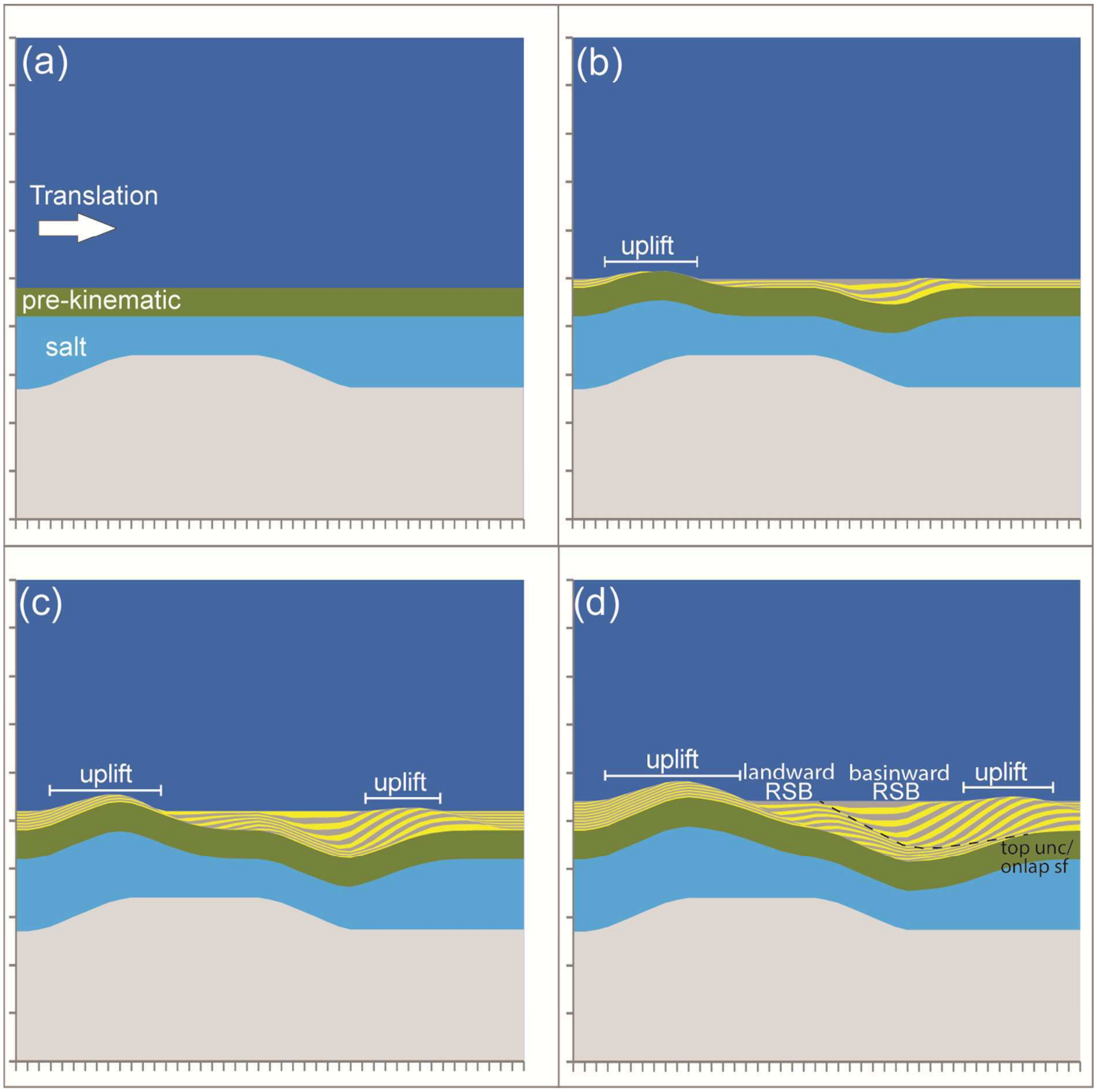

Figure 17: Numerical model showing the sequential evolution (a) to (d) of overburden translation and Couette-type salt flow above two oppositely dipping base-salt ramps and the development of hybrid stacked RSBs.

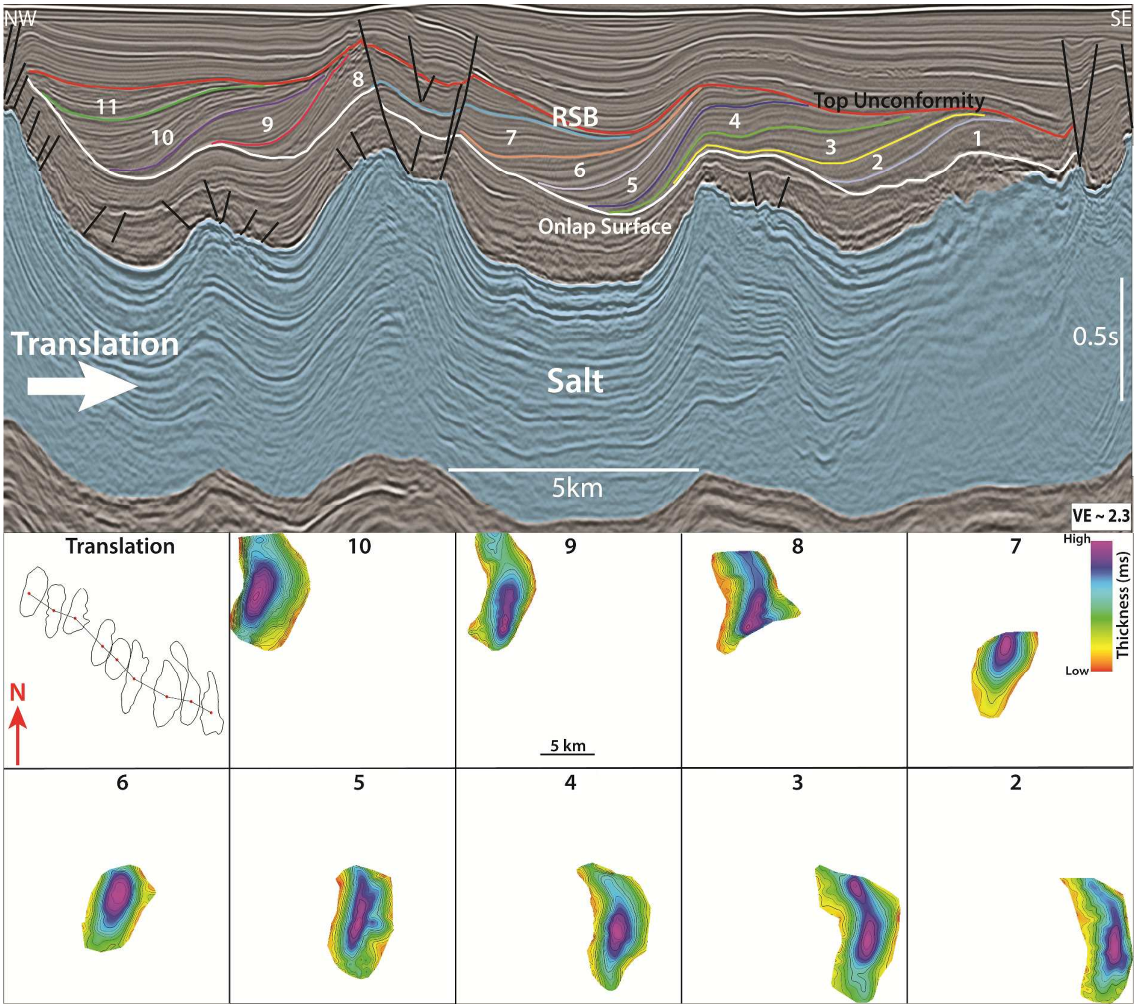

Figure 18: Interpreted seismic section of RSB 5 showing typical landward-dipping sigmoidal intervals and respective thickness maps illustrating the 3D kinematics of the system with 26.9 km of translation towards SE (120 ± 15 azimuth). Oldest intervals are located further downdip of the associated base-salt ramp. Thickness maps of intervals 1 and 11 are not shown because these intervals are affected by a higher degree of salt-related folding and faulting, which hinders the generation of confident maps.

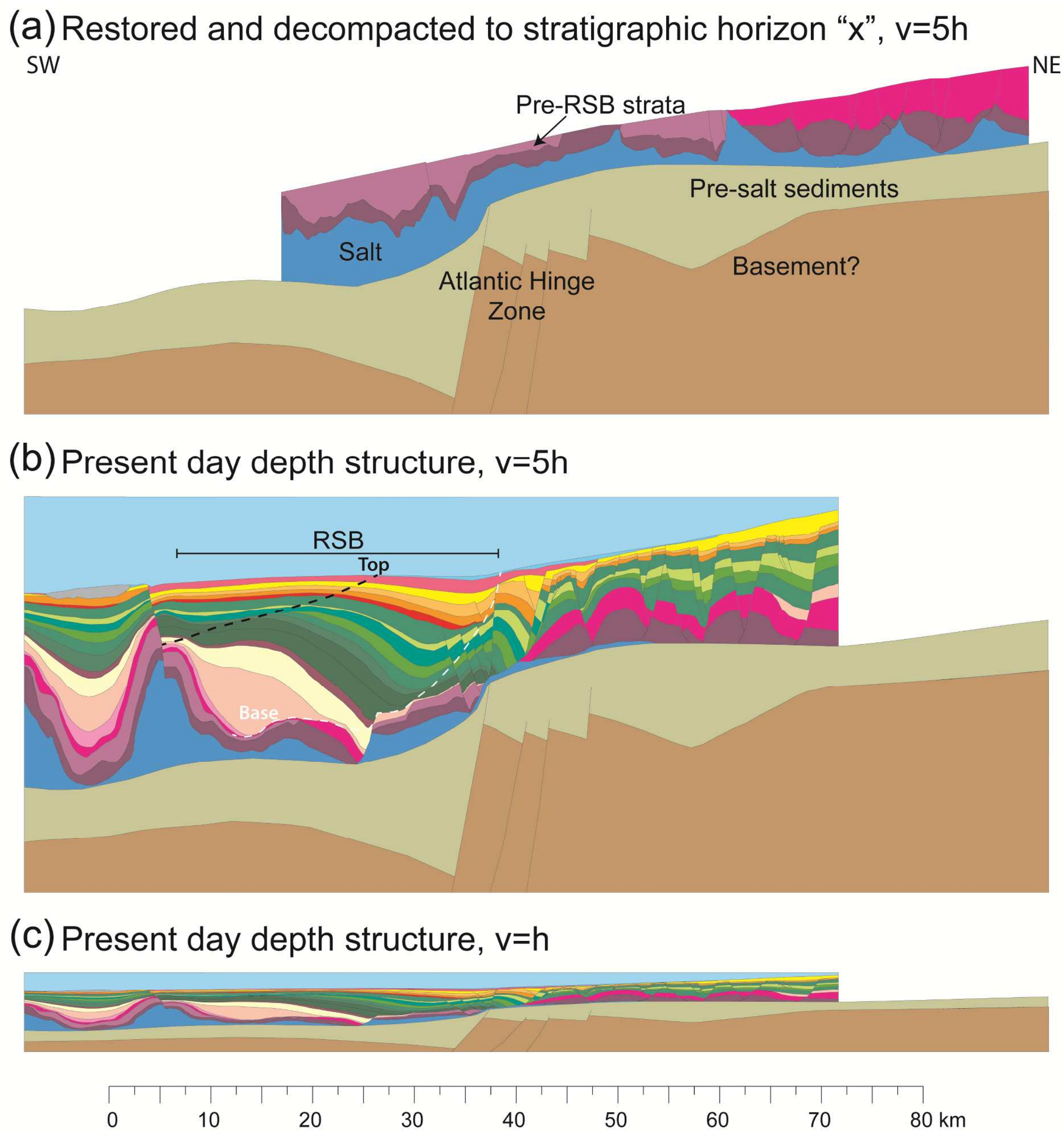

Figure 19: restoration of Line 214 from the Lower Kwanza Basin (adapted from Peel, 2014). Salt is in blue and RSB intervals are represented by colours ranging from purple, green, orange and yellow. RSB forms by translation over the Atlantic Hinge zone, which corresponds to a major basinward-dipping base-salt step. Original salt thickness varies from 1 km above the ramp to 2 km downdip. Translation is ongoing as the system is capped landward by the sea-floor. A total of 24 km of translation has been measured in this section.

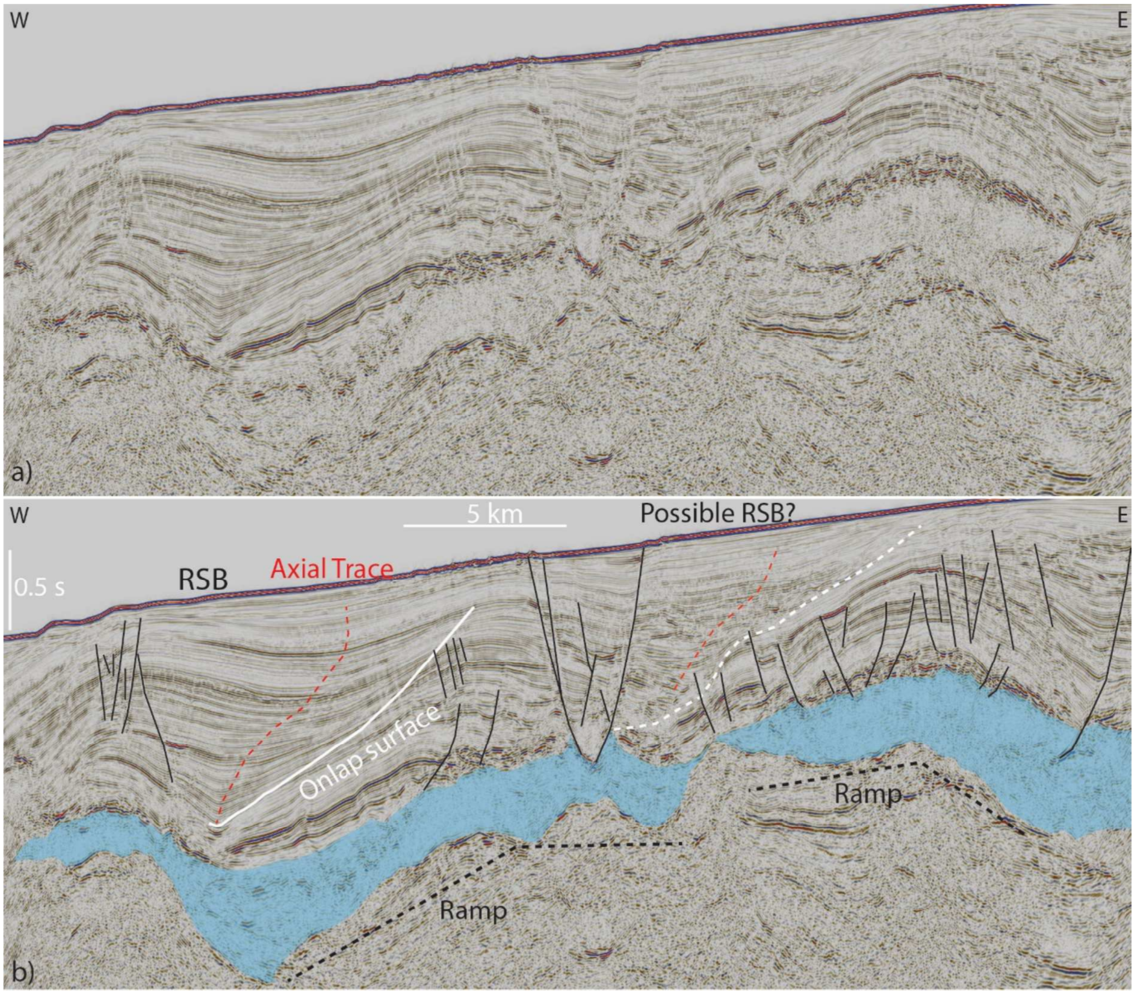

Figure 20: Seismic section showing a simple RSB formed above allochthonous salt (blue) with a base-salt basinward-dipping ramp in the Essaouira-Agadir Basin, Morocco. Another possible candidate of RSB appears to the East but the limited seismic resolution in the area hinders its clear identification.